Suppression of period-doubling and nonlinear parametric effects in periodically perturbed systems

Paul Bryant
Department of Physics, University of California, Berkeley, California 94720
and Materials and Molecular Research Division, Lawrence Berkeley Laboratory, Berkeley, California 94720

Kurt Wiesenfeld
Department of Physics, University of California, Santa Cruz, California 95064
*and Department of Physics, Brookhaven National Laboratory, Upton, New York 11973**
(Received 30 September 1985)

We consider the effect on a generic period-doubling bifurcation of a periodic perturbation, whose frequency ω_1 is near the period-doubled frequency $\omega_0/2$. The perturbation is shown to always suppress the bifurcation, shifting the bifurcation point and stabilizing the behavior at the original bifurcation point. We derive an equation characterizing the response of the system to the perturbation, analysis of which reveals many interesting features of the perturbed bifurcation, including (1) the scaling law relating the shift of the bifurcation point and the amplitude of the perturbation, (2) the characteristics of the system's response as a function of bifurcation parameter, (3) parametric amplification of the perturbation signal including nonlinear effects such as gain saturation and a discontinuity in the response at a critical perturbation amplitude, (4) the effect of the detuning $(\omega_1-\omega_0/2)$ on the bifurcation, and (5) the emergence of a closely spaced set of peaks in the response spectrum. An important application is the use of period-doubling systems as small-signal amplifiers, e.g., the superconducting Josephson parametric amplifier.

I. INTRODUCTION

This paper concerns the effect of periodic perturbations on dynamical systems near the onset of a period-doubling bifurcation. We consider perturbations of a particular sort, which we call "near-resonant:" if the unperturbed system oscillates with fundamental frequency ω_0 and is close to the onset of oscillations at $\omega_0/2$, then a periodic perturbation will be near-resonant if it has frequency ω_1 nearly equal to $\omega_0/2$. Quite generally, near a bifurcation point, one expects a system to be sensitive to even small perturbations. Recently it was shown that systems are *extremely* sensitive to near-resonant perturbations. The first detailed analysis of this sensitivity for period-doubling systems was carried out by Heldstab *et al.* in their work on one-dimensional iterative maps.[1] Later, an analogous theory for systems of differential equations was developed.[2] The theoretical expectations have been experimentally demonstrated using an NMR laser.[3] In the present paper, we examine this sensitivity in great detail, finding a number of interesting phenomena. Our major result is that *near-resonant perturbations suppress the onset of subharmonic oscillations.* Stated differently, we find that the bifurcation point of an unperturbed system is *shifted* due to the presence of the (small) near-resonant perturbation in a way that *stabilizes* the system. The magnitude of the shift depends, of course, on both the amplitude and detuning frequency of the perturbation, where the detuning δ is defined to be $\omega_1-\omega_0/2$. The primary purpose of this paper is to understand theoretically the shift, and to test our theoretical understanding in a quantitative way against measurements made on a nonlinear electrical circuit.

In addition to the shifted bifurcation point, the presence of a near-resonant perturbation induces a number of other interesting effects: for example, the rapid growth of a large number of closely packed lines in the power spectrum near the frequency $\omega_0/2$. A second purpose of this paper is to describe this and other observed features, and to understand them within the framework of a relatively simple theory. This theory is compared with analog simulations in Sec. VI.

The general topic of the effect of small perturbations on systems near the onset of dynamical instabilities—not necessarily period doublings—has a sizable literature devoted to it. Much of the previous work concerned random perturbations. One interesting result is that the bifurcation point, in certain cases, may be a function of the external noise strength.[4] (In these studies a bifurcation of the stochastic system is defined in terms of qualitative changes in the stationary probability density, whose evolution is governed by a Fokker-Planck equation.) The prediction that external noise can shift the bifurcation point away from the value for the corresponding deterministic system has been verified experimentally.[5]

In the case of these so-called noise-induced transitions, instances are known in which noise can either stabilize or destabilize the dynamics. In one example, where a stable fixed point of the noise-free system undergoes a Hopf bifurcation, Hoffmann showed that noisy perturbations can

shift the bifurcation point in either direction, depending on the values of the other parameters in the problem.[6]

Working in a more general framework, Arnold[7] has shown, for linear systems of the form

$$\dot{\mathbf{x}}=\underline{A}(t)\mathbf{x}$$

possessing a fixed point $\mathbf{x}_0$, where $\underline{A}(t)$ is a deterministic matrix, that the addition of a parametric noise term $\underline{B}(t)\mathbf{x}$, with $\underline{B}$ a stochastic matrix, may serve to stabilize an unstable fixed point or destabilize a stable fixed point. Interestingly enough, it has been proven that the proper choice for $\underline{B}$ can *always* serve to stabilize an unstable $\mathbf{x}_0$, provided the trace of $\underline{A}$ is less than zero.[7]

The effect of coherent (i.e., nonrandom) perturbations has also been studied in this vein. For example, it is well-known that the unstable equilibrium point of an inverted pendulum can be stabilized by parametric oscillations.[8] In some recent work, Meerkov[9] has investigated in a more general way the issue of stabilizing systems—linear and nonlinear—by introducing fast parametric oscillations. The goal of that work was to determine the conditions under which "vibrational stabilization" is possible. Other papers on this topic, but with a more specific focus, have also appeared in recent years. Rosenblat *et al.*[10] have analyzed the problem of Bénard convection, when the fluid layer is heated from below in a time-periodic way. They conclude that the periodic component of the heating suppresses the onset of steady convection. That is, if the fluid is heated at the (constant) critical temperature for the onset of convection, the addition of a small, high-frequency temperature oscillation applied at the bottom of the layer stabilizes the subcritical (purely conducting) behavior. More recently, a calculation was made of the response of a one-dimensional nonlinear oscillator subject to a small, parametric (not necessarily periodic) forcing, when the unforced system is near the critical point for a pitchfork bifurcation.[11] Again, the authors conclude that the perturbations tend to stabilize the subcritical behavior.

All of the studies cited above address the general issue of the effect of perturbations on systems that can undergo dynamical instabilities. This is also a major theme of this paper. By way of orienting the reader, we mention that these other works all dealt with bifurcations of time-independent states (i.e., fixed points of the governing differential equations), while this paper focuses on the period-doubling instability, which is a bifurcation from one time-periodic stable state to another. In this regard, work concerning the effect of perturbations on discrete mappings deserves mention,[12] as does previous work on noisy perturbations of continuous periodic systems near the onset of various codimension-one bifurcations.[13,14]

Aside from this general question of how perturbations can affect the stability properties of dynamical systems, we have an additional motivation of a more specific nature. We first came across the phenomena discussed in this paper during an investigation of how period-doubling systems can act as small-signal amplifiers.[2] It was found that a dynamical system poised near the bifurcation point between stable oscillations of fundamental frequency f and $f/2$ will amplify periodic perturbations near frequencies $f/2$, $3f/2$, $5f/2$, etc. (these are perturbations we named "near-resonant" at the beginning of this Introduction). The theory developed in Refs. 1 and 2—which also predicts that a similar phenomenon exists for other types of bifurcations of periodic orbits—is based on a linearized perturbation theory which assumes that the bifurcation point for the onset of oscillations at $f/2$ is *unshifted* in the presence of the small-signal perturbation. (Nonlinear effects were also considered in Ref. 1, for the specific case where the linear response vanishes—i.e., precisely at the bifurcation point—and the detuning is zero. The issue of a shifted bifurcation point is not addressed in that work.) While analog simulations agree well with the theory for small enough signals, for larger perturbations the shift of the bifurcation point cannot be ignored. One of the purposes of this paper, then, is to understand the amplification mechanism of Refs. 1 and 2 more fully. An important application of these ideas concerns the operation of superconducting Josephson-junction parametric amplifiers, as will be discussed in Sec. VII. The understanding gained in this paper may provide an important clue to the long-standing problem of the anomalous noise rise observed in those devices.

II. OVERVIEW OF RESULTS

In this section we give an overview of our results, emphasizing their consequences, and providing some motivation for the approach taken in this work.

A. Theoretical results

We are interested in obtaining a general equation that describes the dynamics of a system which is near the onset of a period-doubling bifurcation and is subject to a near-resonant perturbation. The general equation we derive is a normal form,[15] i.e., it applies to a broad class of systems. This class includes all generic (or nondegenerate) systems which exhibit a period-doubling bifurcation of the supercritical type, i.e., those in which a *stable* period-doubled orbit emerges from the original orbit beyond the bifurcation point, and which are subjected to a sinusoidal perturbation. The general system of this type will follow the normal form exactly only in the limit of small perturbation amplitude and detuning, where higher-order terms can be neglected. We assume ω_0 (the fundamental frequency) and ω_1 (the perturbation frequency) are both fixed and not subject to any phase-locking phenomena; in other words, the unperturbed system is considered to be nonautonomous, presumably as a result of a periodic forcing at frequency ω_0.

For a system near the onset of a period-doubling instability, the dynamics can be broken down into several components, which have different time scales during which they are of importance. First there is the periodic orbit which is going unstable. We represent this by $\mathbf{X}_0(\theta)$ where $\theta=\omega_0 t$, so $\mathbf{X}_0(\theta)$ is a periodic function of θ with period 2π. The system is soft in one direction in phase space due to the period-doubling instability but presumed strongly stable (by comparison) in all other directions. These stable directions have a very short time scale associated with them (for transient decay) and will be complete-

ly ignored. Conversely, transients associated with the period doubling have a very long decay time (many cycles of ω_0). These are represented by a period-doubled oscillation $\mathbf{X}_1(\theta/2)$ with a period of 4π in θ, whose amplitude may be slowly varying in time. How the amplitude varies will depend on the bifurcation parameter and on the perturbation term. We call the amplitude of this period-doubled term the reduced scalar variable x. Thus the dynamical variable $\mathbf{X}$ can be expressed in terms of x as

$$\mathbf{X}=\mathbf{X}_0(\theta)+x\mathbf{X}_1(\theta/2)\ , \tag{1}$$

where $\theta=\omega_0 t$, $\mathbf{X}_0(\theta)=\mathbf{X}_0(\theta+2\pi)$, and $\mathbf{X}_1(\theta/2)=-\mathbf{X}_1((\theta+2\pi)/2)$.

In Sec. III A we will derive the "reduced equation" for $\dot{x}$, which is

$$\dot{x}=\mu x-x^3+\epsilon\cos(\delta t)\ , \tag{2}$$

where μ is a bifurcation parameter (defined so that $\mu=0$ is the unperturbed bifurcation point), ϵ is the perturbation amplitude (assumed positive), and $\delta\equiv\omega_1-\omega_0/2$ is the "detuning" of the perturbation frequency. This equation is the normal form which governs the dynamics of the perturbed bifurcation in nondegenerate cases.

Consider the case $\epsilon=0$ (no perturbation). Then Eq. (2) is the normal form for a symmetry-breaking bifurcation; $x=0$ is the stable fixed point for $\mu<0$, while $x=\pm\sqrt{\mu}$ are stable fixed points for $\mu>0$. This bifurcation in x results in the period doubling of $\mathbf{X}$ for $\mu>0$. Now consider the case $\epsilon\neq 0$ (perturbation present). Since the term $\epsilon\cos(\delta t)$ appears in Eq. (2), there can be no fixed points for x and the attracting solution must be a limit cycle. In Sec. III D we show that $x(t)$ is a symmetric oscillation [i.e., $x(t)=-x(t+\pi/\delta)$] below the shifted bifurcation point μ_B, after which it undergoes a symmetry-breaking bifurcation. The presence of a constant component to $x(t)$ for $\mu>\mu_B$ results in the appearance of $\omega_0/2$ in the frequency spectrum of $\mathbf{X}$, heralding the onset of period doubling, as is discussed in Sec. III E.

By studying Eq. (2) a number of important results are obtained. A change of variables can eliminate one of the parameters (either ϵ, δ, or μ). From this we obtain scaling relations, the most important of which is the shift power law: $\mu_B\propto\epsilon^{2/3}$ in the limit of small δ as discussed in Sec. III C. This relation remains true for nonsinusoidal perturbations as well. The bifurcation shift μ_B is in general a function of δ and ϵ, and in Fig. 1 we show a projected view of this function, which was determined numerically. Note that μ_B increases with ϵ and decreases with δ (but is always >0). Rescaling the equation allows one to study the behavior in a two- (rather than three-) dimensional parameter space as we do for all other figures in this paper.

In order to better understand the dynamics of the nonlinear reduced equation [Eq. (2)], we use a combination of two approaches: (1) the generation of analytic solutions for a variety of limiting cases, such as large μ or large δ (see Sec. III F); and (2) the numerical determination of certain features, such as the bifurcation shift, in the parameter regions where the nonlinearities are not small.

In Sec. IV we explore in detail the behavior in the limit of small detuning. We call this the "quasistatic regime"

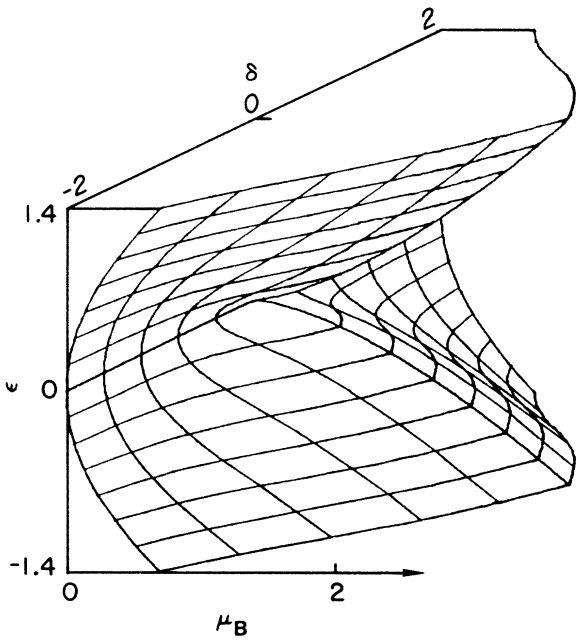

FIG. 1. Bifurcation shift μ_B as a function of detuning δ and perturbation amplitude ϵ. Determined numerically from Eq. (2).

because the reduced variable $x(t)$ has a nearly zero time derivative. When the operating point is between the original and shifted bifurcation points, the quasistatic description breaks down for brief intervals during which there is a rapid transition in $x(t)$ followed by another long period of slow quasistatic change. The result is a symmetrical square-wave-like oscillation for $x(t)$. This behavior is easily observed experimentally, especially in a Poincaré section, i.e., a periodically strobed phase portrait. The squareness of $x(t)$ has important consequences for the frequency spectrum, generating an *evenly spaced* set of peaks which is centered on $\omega_0/2$ (or an odd harmonic of $\omega_0/2$) and which falls off *symmetrically* on either side. (We would like to suggest the name "menorah" for this type of spectrum, due to its resembling a menorah or candelabrum.) Another important feature of the quasistatic regime is that there is a discontinuous change in the attracting solution for $x(t)$ at the bifurcation point. This discontinuity is seen in the amplitudes of all the spectral components. The $\omega_0/2$ component jumps from zero to a finite value, while the ω_1 component drops by a factor of $2\sqrt{7}$. We plot the behavior of these two components over a range of parameter values in Sec. IV B. This plot shows that the ω_1 response reaches a maximum slightly before the shifted bifurcation point, and that the $\omega_0/2$ response continues to increase beyond its initial jump at the bifurcation point. The discontinuity is also observed when varying the perturbation amplitude ϵ. This is because the bifurcation shift varies with ϵ, and for any $\mu>0$ there is a critical ϵ above which the bifurcation is suppressed. Thus the parametric gain of the perturbation signal can (under certain conditions) be highly nonlinear, containing a *switchlike discontinuity*. Further discussion of this effect can be found in Secs. IV B and VII.

When the detuning is large enough to be significant, we

enter the "dynamic regime" which is the subject of Sec. V. The bifurcation that occurs in the quasistatic limit is of a very degenerate nature—$x(t)$ undergoes a discontinuous change at the bifurcation point. For nonzero detuning, however, this degeneracy is eliminated and we expect a generic (or typical) symmetry-breaking bifurcation of the reduced variable $x(t)$, resulting in a period doubling of the dynamical variable $\mathbf{X}(t)$. As the detuning is decreased, we find that the behavior rapidly approaches the discontinuous behavior of the quasistatic approximation; i.e., near the bifurcation point one finds that $x(t)$ changes in a very rapid and nearly discontinuous way with bifurcation parameter. In fact this change can be so rapid and occur over so small a parameter interval as to be indistinguishable for all practical purposes from a true discontinuity in an experimental system.

In the dynamic regime there are several important functions of the detuning which can be determined from the reduced equation. We study three such functions. (1) The shifted bifurcation point—this is perhaps the most important feature in the parameter space, especially for small detuning where $x(t)$ undergoes a nearly discontinuous change. (2) The bifurcation "width"—defined in Sec. V B, this is inversely related to the rapidity with which $x(t)$ changes near the bifurcation point, and serves as a guide to which levels of detuning will lead to the quasistatic-discontinuous type of behavior in an experimental system of finite resolution and noise. (3) Maximum gain—this is the point at which the response at the perturbation frequency ω_1 is at a maximum. It is a very important feature to know for a period-doubling system that is being used as an amplifier. The maximum always occurs between the original and shifted bifurcation points.

For intermediate values of the detuning, these three functions are studied numerically and plotted, while asymptotic expressions are derived analytically for large detunings. All three curves fall off like δ^{-2} in this asymptotic region. One interesting feature of these curves is their behavior near zero detuning: the bifurcation shift curve has a pointed peak with a discontinuous derivative; the maximum gain curve has a cusp at $\delta=0$; and the bifurcation width goes to zero extremely rapidly as δ decreases, roughly like $\exp(-1/\delta)$.

B. Analog simulations

As a preliminary test of the theoretical results we made measurements on a simple period-doubling system: the forced Duffing's equation generated by an analog simulator. We present the detailed results of this study in Sec. VI.

The simulator is a precision electronic circuit from which data was taken using standard electronic test equipment including a spectrum analyzer. Some of our reasons for choosing this system over a more complex experimental system are (1) very low stochastic noise level, (2) high level of reproducibility, and (3) the possibility that some results might be derived analytically for the Duffing equation (this has not yet been done except for the linearized behavior[1]).

The simulator was used to check several results of the theory. (1) The shift power law was checked by plotting measured values of the bifurcation point as a function of the perturbation amplitude for very small detuning on a log-log scale. The results show excellent agreement with the predicted $\frac{2}{3}$ power law. (2) The system response at the perturbation frequency was measured on a spectrum analyzer for a sequence of bifurcation parameter settings. This was done with very small detuning and constant perturbation amplitude. The results were rescaled for a best fit with the theoretical curve for the quasistatic regime, given in Sec. IV B. The agreement is excellent, particularly below the shifted bifurcation point. (3) The bifurcation shift was measured for a sequence of detuning values. These values were rescaled and compared with the theoretical plot given in Sec. V B. Again the agreement was found to be excellent—particularly the matching of the pointed peak feature. (4) Spectra were generated corresponding to the three special cases (all in the quasistatic regime) which are calculated analytically in the Appendix. These all show the symmetrical set of evenly spaced peaks mentioned previously. The agreement with theory in all cases is quite good, although there is some deviation of the higher-order peaks due to the nonzero detuning used.

In addition to these simulations, a few qualitative observations were made on a more complex system: a forced magnetic oscillator, described in a previous work.[16] The system had to be modified slightly by adding a constant term to the forcing and changing from a negative to a positive damping. This encouraged period doubling and discouraged the Hopf bifurcation which was the main focus of the previous study. We made only qualitative observations on this system. A shift was easily observed in the bifurcation point which occurred in the predicted direction, suppressing the bifurcation. We also observed the square-wave behavior of $x(t)$, which is predicted to occur between the original and shifted bifurcation points for small detuning (quasistatic regime). However, for reasons discussed previously, we decided to take accurate measurements using simulations rather than this more complex system.

III. THE PERTURBED BIFURCATION

A. Derivation of reduced flow (normal form)

In this section we give a detailed derivation of Eq. (2) (the normal form). First we will review a linearized Floquet analysis[17] of the unperturbed system and then show how this can be modified to include the influence of the dominant nonlinear term and of the perturbation. For the unperturbed system, we assume the dynamics are governed by a differential equation of the form

$$\dot{\mathbf{X}}=\mathbf{F}(\mathbf{X},\theta,\mu)\ , \tag{3}$$

where $\mathbf{X}\in\mathbb{R}^n$, $\theta=\omega_0 t$, and μ is a bifurcation parameter. We assume $\mu=0$ is the bifurcation point and that near this point exists a periodic solution to Eq. (3): $\mathbf{X}=\mathbf{X}_0(\theta,\mu)$, which satisfies $\mathbf{X}_0(\theta,\mu)=\mathbf{X}_0(\theta+2\pi,\mu)$ and is asymptotically stable for $\mu<0$. At $\mu=0$ we assume a *supercritical*[18] period-doubling bifurcation of this orbit, so that for $\mu>0$, $\mathbf{X}_0$ is an unstable orbit and there is a coex-

isting stable period-doubled orbit.

The behavior of transients near $\mathbf{X}_0$ can be studied by Floquet analysis. Define

$$\boldsymbol{\eta} \equiv \mathbf{X} - \mathbf{X}_0(\theta,\mu) \ . \tag{4}$$

By linearizing Eq. (3), it follows that

$$\dot{\boldsymbol{\eta}} \approx D\underline{F}(\mathbf{X}_0)\cdot\boldsymbol{\eta} \tag{5}$$

where $(D\underline{F})_{ij} = \partial F_i/\partial X_j \,|_{\mathbf{X}=\mathbf{X}_0}$. Note that $(D\underline{F})_{ij}$ is periodic in θ.

Floquet theory shows that the solution to this equation can be reduced to

$$\boldsymbol{\eta} = \sum_k z_k \mathbf{Z}_k(\theta) \ , \tag{6}$$

where z_k is a complex scalar satisfying

$$\dot{z}_k = \rho_k z_k \tag{7}$$

and $\mathbf{Z}_k(\theta)$ is a periodic function of θ. The ρ_k are called the Floquet exponents. In general, ρ_k, z_k, and $\mathbf{Z}_k$ may be complex while $\boldsymbol{\eta}$ must be real since $\mathbf{X}$ is real.

When near a period doubling, one of the exponents, say ρ_1, is of the form $\mu + i\omega_0/2$ where μ is real and small. In this case $\mathbf{Z}_1$ must be of the form

$$\mathbf{Z}_1(\theta) = e^{-i\theta/2}\mathbf{X}_1(\theta/2) \ , \tag{8}$$

where $\mathbf{X}_1(\theta/2)$ is a real function satisfying

$$\mathbf{X}_1((\theta/2)+\pi) = -\mathbf{X}_1(\theta/2) \ . \tag{9}$$

We assume that the other Floquet exponents are strongly stable compared to ρ_1, having negative real parts. The terms corresponding to these exponents in Eq. (7) will therefore decay rapidly and can be ignored. Thus we find

$$\mathbf{X}(\theta/2,x) = \mathbf{X}_0(\theta) + x\mathbf{X}_1(\theta/2) \ , \tag{10}$$

where x is a real *scalar* satisfying $\dot{x} = \mu x$.

We are now ready to extend this analysis to include nonlinear effects and the influence of a near-resonant perturbation. Equation (10) is effectively a reduction of the dynamics to the center manifold[15] for the period doubling. For this case, the important dynamics occur on a two-dimensional surface with a Möbius-strip-like character (i.e., a band with a half-twist in it) which includes the central orbit $\mathbf{X}_0(\theta)$. The scalar x may be thought of as a transverse coordinate on the strip which is zero on the central orbit. The dynamics of motion on this surface are governed by the equation for $\dot{x}$. Nonlinear and perturbation terms in the full dynamical equation will introduce similar terms into the equation for $\dot{x}$. We are not interested in other effects of nonlinearities, such as curvature of the center manifold, because these effects will be small as long as $x\mathbf{X}_1$ is small compared to $\mathbf{X}_0$. A general expression for $\dot{x}$ is thus

$$\dot{x} = \mu x + f_{\rm NL}(x,\theta/2) + \epsilon g(x,\theta/2)\cos(\omega_1 t) \ , \tag{11}$$

where $f_{\rm NL}(x,\theta/2)$ is the nonlinear dependence of $\dot{x}$ on x and $g(x,\theta/2)$ gives a linear approximation of the influence of the perturbation $\epsilon\cos(\omega_1 t)$ on $\dot{x}$. The functions $f_{\rm NL}$ and g depend on $\theta/2$ rather than θ only because of the transformation we made via Eq. (8) in order to obtain all real quantities. Since $\mathbf{X}(\theta/2,x)$ and $\mathbf{X}((\theta+2\pi)/2,-x)$ are the same point in phase space [see Eqs. (9) and (10)], the values of $f_{\rm NL}$ and g must have the symmetry

$$f_{\rm NL}(x,\theta/2) = -f_{\rm NL}(-x,(\theta/2)+\pi) \ , \tag{12}$$

$$g(x,\theta/2) = -g(-x,(\theta/2)+\pi) \ . \tag{13}$$

We now average[15] the equation for $\dot{x}$ over two periods of ω_0. Because of symmetry the quadratic (in x) component of $f_{\rm NL}$ is eliminated by this averaging process so that the dominant nonlinearity is cubic:

$$\dot{x} = \mu x - x^3 + \epsilon g_{\rm av}(x,\delta t) \ , \tag{14}$$

where

$$\begin{aligned} g_{\rm av}(x,\delta t) &= (\omega_0/4\pi)\int_t^{t+4\pi/\omega_0} g(x,\omega_0 t'/2)\cos(\omega_1 t')dt' \\ &\approx (1/4\pi)\int_0^{4\pi} g(x,\theta'/2)\cos(\tfrac{1}{2}\theta' + \delta t)d\theta' \end{aligned}$$

and $\delta = \omega_1 - \omega_0/2$ is the detuning of the perturbation frequency. The coefficient of x^3 can always be made equal to -1 as in Eq. (14) by an appropriate choice of scale for x. The scale factor is incorporated into the definition of $\mathbf{X}_1(\theta/2)$. The sign of the x^3 term must be negative for a supercritical bifurcation.

Under conditions where $x(t)$ is of sufficiently small magnitude, it is a reasonable approximation to replace $g_{\rm av}(x,\delta t)$ with $g_{\rm av}(0,\delta t)$. We can clarify this with a change of variables. Let $x_1 = x/\epsilon^{1/3}$ and $t_1 = \epsilon^{2/3}t$. Substituting these into Eq. (14) we obtain

$$\frac{dx_1}{dt_1} = \mu_1 x_1 - x_1^3 + g_{\rm av}(\epsilon^{1/3}x_1,\delta_1 t_1) \ , \tag{15}$$

where $\mu_1 = \mu/\epsilon^{2/3}$ and $\delta_1 = \delta/\epsilon^{2/3}$.

We now wish to consider the limit of small perturbation $\epsilon \to 0$ with μ_1 and δ_1 fixed. In this limit $g(\epsilon^{1/3}x_1,\delta_1 t_1) \to g(0,\delta_1 t_1)$. This is the case we will be discussing for the remainder of the paper, i.e., what are the properties of this perturbed bifurcation in the limit of small perturbations?

The expression for $g_{\rm av}(0,\delta t)$ can be simplified: Define

$$\tilde{g} \equiv (1/4\pi)\int_0^{4\pi} g(0,\theta'/2)e^{i\theta'/2}d\theta' \ ,$$

then

$$\begin{aligned} g_{\rm av}(0,\delta t) &= (e^{i\delta t}\tilde{g} + e^{-i\delta t}\tilde{g}^*)/2 \\ &= |\tilde{g}|\cos(\delta t + \delta_0) \ , \end{aligned} \tag{16}$$

where $\delta_0 = \arg(\tilde{g})$. The factor $|\tilde{g}|$ can be set to unity by appropriate definition of ϵ, and δ_0 can be set to zero by appropriate choice for $t=0$. Thus x satisfies $\dot{x} = \mu x - x^3 + \epsilon\cos(\delta t)$, which is what we set out to prove in this section, i.e., this is Eq. (2), the normal form. Note: for non-sinusoidal perturbations odd harmonics of $\epsilon\cos(\delta t)$ may appear in the normal form.

B. Dynamics in the Poincaré section

The dynamics of the reduced variable $x(t)$ is related to the behavior of the Poincaré map[15] for the system. Sup-

pose the initial intersection of the orbit with the Poincaré (surface of) section occurs at time t_0 where $\mathbf{X}=\mathbf{X}_{(0)}$. Then from Eq. (1), the nth iterate of this point (i.e., the point n cycles later) is given by

$$\mathbf{X}_{(n)}=\mathbf{X}_0(\theta_0)+(-1)^n x(t_n)\mathbf{X}_1(\theta_0/2)\ , \tag{17}$$

where $\theta_0=\omega_0 t_0$ and $t_n=t_0+2\pi n/\omega_0$. Since the vectors $\mathbf{X}_0(\theta_0)$ and $\mathbf{X}_1(\theta_0/2)$ do not depend on the iteration n, the important dynamics in the Poincaré section are *one dimensional.* As a result of this, the sequence of points in the Poincaré section all fall (approximately) on a straight line in the Poincaré section, and the motion on this line is governed by the *slowly* varying $x(t_n)$. Below the bifurcation point the attractor is a single line segment, while above the bifurcation point, there is a back and forth iteration between points on two line segments. In the latter case, both segments are constrained to lie on the same straight line mentioned previously. For some small parameter interval past the bifurcation point, these segments will overlap, appearing as one segment. (They are easily separated, however, by strobing every other cycle.) The point beyond which these segments no longer overlap is called the *separation point* and is discussed further in Sec. V C. Note: the line segments are actually limiting cases of highly eccentric elipses; the eccentricity results from the close proximity of the period-doubling instability.

C. Rescaling the equation—shift power law

In a previous subsection, we derived Eq. (2), the reduced equation governing the dynamics of the perturbed bifurcation. This equation depends on the three parameters in the problem: the bifurcation parameter μ, the perturbation amplitude ϵ, and the detuning δ. However, it is possible to eliminate one parameter by rescaling the equation. This is particularly useful for doing numerical studies of the equation, since a reduction in the dimension of the parameter space greatly reduces the number of data points needed to survey the behavior of the equation, as well as making it much easier to display the results. There are several ways in which the rescaling may be accomplished; we consider two of these. In the first of these forms, ϵ is eliminated, while in the second μ is eliminated. Subscripts 1 and 2 denote the parameters and variables of the first and second forms, respectively.

The first rescaling form is

$$\frac{dx_1}{dt_1}=\mu_1 x_1-x_1^3+\cos(\delta_1 t_1)\ , \tag{18}$$

where $x_1=x/\epsilon^{1/3}$, $t_1=t\epsilon^{2/3}$, $\mu_1=\mu/\epsilon^{2/3}$, and $\delta_1=\delta/\epsilon^{2/3}$. This form is particularly useful when studying the situation where ϵ is a fixed parameter because then μ_1 and δ_1 are linearly dependent on the parameters being varied, i.e., $\mu_1\propto\mu$ and $\delta_1\propto\delta$. Numerical studies of this equation are to be found in both Secs. IV and V and are compared with the results of analog simulations in Sec. VI.

From the rescaling that resulted in Eq. (18) we can immediately determine some important scaling laws. This is because it is possible to find ways to change the original parameters (ϵ, μ, and δ) which leaves the new parameters μ_1 and δ_1 unchanged and therefore results in similar dynamics. The way to do this is to maintain μ and δ proportional to $\epsilon^{2/3}$. From this fact one can obtain scaling rules for specific features of interest. If μ_B is the location of the shifted bifurcation point, then it obeys the shift power law

$$\mu_B\propto\epsilon^{2/3} \tag{19}$$

under the condition that either δ is insignificantly small (this is the quasistatic case—see Sec. IV) or that δ is also kept proportional to $\epsilon^{2/3}$. This effect is easy to observe in experimental systems and was accurately verified by our analog simulations of Duffing's equation (see Sec. VI).

The second form for rescaling the equation is

$$\frac{dx_2}{dt_2}=\mathrm{sgn}(\mu)x_2-x_2^3+\epsilon_2\cos(\delta_2 t_2)\ , \tag{20}$$

where $x_2=x/|\mu|^{1/2}$, $t_2=t|\mu|$, $\epsilon_2=\epsilon/|\mu|^{3/2}$, $\delta_2=\delta/|\mu|$, and $\mathrm{sgn}(\mu)$ is the sign (or signum function) of μ. This form is particularly useful for cases where the bifurcation parameter μ is held fixed. The fact that the form of the equation depends on the sign of μ results from the fact that the sign of t_2 must be the same as t. These two cases show distinctly different behavior, but this should be expected since $\mu=0$ is the unperturbed bifurcation point.

In this paper we emphasize the behavior of the first form [Eq. (18)] over that of the second form [Eq. (20)], since one of our main goals is to understand the nature of the bifurcation shift. The second form is analyzed in detail for the quasistatic case in Sec. IV, where we examine nonlinearities of the response as a function of ϵ. However, the reader should be aware that in other sections of the paper where the second form is not discussed, results given for the first form in terms of μ_1 can be converted to the corresponding results for the second form by the transformation $\epsilon_2=|\mu_1|^{-3/2}$, $\delta_2=\delta_1/|\mu_1|$, and $x_2=x_1/|\mu_1|^{1/2}$.

D. Stabilizing effect of the perturbation

For one-dimensional forced systems of the form $\dot{x}=f(x,t)$, the stability of a T-periodic orbit may be found by computing $\int_0^T(\partial\dot{x}/\partial x)dt$ along the orbit. If this integral is positive, then deviations from the orbit will grow, i.e., it is an unstable orbit, while a negative result implies stability. From Eq. (2),

$$\frac{\partial\dot{x}}{\partial x}=\mu-3x^2\ . \tag{21}$$

Even without having an explicit solution for the periodic orbit $x(t)$, a number of conclusions regarding its stability can be drawn. Clearly, for $\mu<0$ any orbit must be stable, since $\mu-3x^2<0$ for all x. Furthermore there can be only one such periodic orbit and it must have the symmetry $x(t)=-x(t+\pi/\delta)$. This follows from the inversion symmetry of Eq. (2)—an asymmetrical orbit $x_+(t)$ always has a complementary form $x_-(t)$ such that $x_-(t)=-x_+(t+\pi/\delta)$, but two stable solutions cannot coexist since they would have to be separated by an unstable or-

bit, and these are not allowed for $\mu<0$.

For $\mu=0$ the unperturbed solution $x=0$ is on the verge of instability since $\mu-3x^2=0$. However, the perturbed solution is an oscillatory function of x, and $\oint \partial\dot{x}/\partial x\, dt$ will still be negative for $\mu=0$ since $\mu-3x^2\leq 0$ for all x. Thus the bifurcation point, where the symmetrical oscillation $x_s(t)$ becomes unstable, will be shifted to some new bifurcation point μ_B which is greater than 0. Numerical studies indicate that for $\mu<\mu_B$ the only solution is $x_s(t)$, while for $\mu>\mu_B$ there are three solutions: $x_s(t)$, which is unstable, and a complementary pair of asymmetrical orbits $x_+(t)$ and $x_-(t)$, which are stable and emerge from x_s at $\mu=\mu_B$ in a symmetry-breaking bifurcation. These two solutions (x_+ and x_-) correspond to the two possible phases of the actual period-doubled orbit $\mathbf{X}(t)$.

E. Frequency spectra

From Eq. (1), $\mathbf{X}=\mathbf{X}_0(\theta)+x\mathbf{X}_1(\theta/2)$. We Fourier decompose $\mathbf{X}_0$ and $\mathbf{X}_1$ as

$$\mathbf{X}_0(\theta)=\sum_n a_n e^{in\omega_0 t}, \tag{22}$$

where $a_n=(1/2\pi)\int_0^{2\pi}\mathbf{X}_0(\theta)e^{-in\theta}d\theta$, and

$$\mathbf{X}_1(\theta/2)=\sum_{n\ \text{odd}} b_n e^{in\omega_0 t/2}, \tag{23}$$

where $b_n=(1/4\pi)\int_0^{4\pi}\mathbf{X}_1(\theta/2)e^{-in\theta/2}d\theta$.

For n even, $b_n=0$ because of the symmetry $\mathbf{X}_1(\theta/2)=-\mathbf{X}_1((\theta/2)+\pi)$. The attracting solution for $x(t)$ will always have period $2\pi/\delta$ and so it can be expressed as

$$x(t)=\sum_m c_m e^{im\delta t}, \tag{24}$$

where $c_m=(\delta/2\pi)\int_0^{2\pi/\delta}x(t)e^{-im\delta t}dt$. Thus the complete spectrum of $\mathbf{X}$ is given by

$$\mathbf{X}(t)=\sum_n a_n e^{in\omega_0 t}+\sum_{\substack{n\ \text{odd},\\ m}} b_n c_m e^{i[n(\omega_0/2)+m\delta]t} \tag{25}$$

For every odd multiple n of $\omega_0/2$ there will be a group of closely spaced peaks at frequencies

$$\omega_{nm}=n(\omega_0/2)+m\delta,\ n\ \text{odd}. \tag{26}$$

As will be shown later, the amplitudes fall off with increasing $|m|$ forming a symmetrical structure of evenly spaced peaks of decreasing heights away from the center. Below the bifurcation point $x(t)$ is a symmetrical oscillation satisfying $x(t)=-x(t+\pi/\delta)$. This has only odd harmonics, suppressing all even values of m in Eqs. (24)–(26). In particular, the central peak in the spectrum, which is $\omega_0/2$ (or a harmonic of $\omega_0/2$), is not present below the bifurcation point. Above the bifurcation point there is a pair of complementary asymmetrical attractors, corresponding to the two possible phases of the period-doubled response. The asymmetry results in a complete spectrum with all m values allowed. The presence of a constant component to $x(t)$ results in the appearance of $\omega_0/2$ in the spectrum of $\mathbf{X}(t)$ since b_1c_0 in Eq. (25) is no longer zero.

This type of spectrum only occurs when $|\mu_1|$ is not large. For $\mu_1\to-\infty$ the reduced response $x(t)$ is approximately sinusoidal (see Sec. III F 1) and thus only c_1 and c_{-1} ($c_1=c_{-1}^*$) are significant. Thus there will be only two peaks near $\omega_0/2$: $\frac{1}{2}\omega_0+\delta$ (this is ω_1, the perturbation or signal frequency) and $\frac{1}{2}\omega_0-\delta$ (sometimes called the idler). The behavior is similar for $\mu_1\to+\infty$ (see Sec. III F 2) except for the addition of the $\omega_0/2$ peak itself.

F. Limiting cases of the normal form and their solutions

We will now examine certain limiting cases of the normal-form equation for which the nonlinearity may be treated as small. The analytic solutions we determine here will later be used to study the asymptotic behavior of several features of interest such as the bifurcation shift.

1. Prebifurcation limit ($\mu/\epsilon^{2/3}\to-\infty$)

For μ_1 sufficiently negative, the cubic term in Eq. (18) can be neglected. Since $\mu_1=\mu/\epsilon^{2/3}$, we are interested in the limit $\mu/\epsilon^{2/3}\to-\infty$. In terms of the original variable and parameters of Eq. (2), we obtain the linear equation

$$\dot{x}=\mu x+\epsilon\cos(\delta t). \tag{27}$$

This can be solved exactly:

$$x(t)=\frac{\epsilon}{\delta^2+\mu^2}[\delta\sin(\delta t)-\mu\cos(\delta t)]. \tag{28}$$

Thus the response is linear in the perturbation amplitude ϵ. The behavior in this limit has been studied previously[1,2] and will not be discussed further here.

2. Postbifurcation limit ($\mu/\epsilon^{2/3}\to\infty$)

Here we make a linear approximation to $\mu x-x^3$ using its derivative evaluated at the zero which occurs at $x=\pm\mu^{1/2}$, thus

$$\mu x-x^3\approx-2\mu x\pm 2\mu^{3/2}. \tag{29}$$

Substituting this into Eq. (2) we obtain

$$\dot{x}=-2\mu x\pm 2\mu^{3/2}+\epsilon\cos(\delta t). \tag{30}$$

The solution to this equation is

$$x(t)=\pm\mu^{1/2}+\frac{\epsilon}{\delta^2+4\mu^2}[\delta\sin(\delta t)+2\mu\sin(\delta t)]. \tag{31}$$

Thus we see that the response is linear in ϵ as in the prebifurcation limit, but now there is also the constant term $\pm\mu^{1/2}$.

3. High-detuning limit ($\delta_1\to\infty$)

a. $\mu_1<\mu_{1B}$. Here we are interested in behavior in the limit $\delta_1\to\infty$ (or $\delta/\epsilon^{2/3}\to\infty$) with μ_1 small, of order δ_1^{-2}, and less than the bifurcation value μ_{1B}. In this regime the solution to $\dot{x}_1=\mu_1x_1-x_1^3+\cos(\delta_1t_1)$ is approximately

$$x_1(t)\approx\frac{1}{\delta_1}\sin(\delta_1t_1) \tag{32}$$

since μ_1x_1 and x_1^3 are both much less than $\cos(\delta_1t_1)$ for

almost all of the orbit. However, we would like to improve this solution obtaining the lowest-order correction due to the $\mu_1 x_1$ and x_1^3 terms (we will actually use the result to study the asymptotic behavior of the maximum gain in Sec. V D). Although we only wish to determine the corrections to the fundamental Fourier component of the solution, the presence of the nonlinearity means there can be coupling between this component and the higher harmonics. The most significant higher harmonic is the third harmonic, i.e., $\cos(3\delta t)$ and $\sin(3\delta t)$. These couple through the cubic term to the $\sin(\delta t)$ and $\cos(\delta t)$ components by cross-multiplying with $1/\delta\sin(\delta t)$ [the approximate solution for $x(t)$ which is much larger than the corrections]. Thus we expand $x(t)$ as

$$x_1(t_1)=(1/\delta_1)\sin(\delta_1 t_1)+a\sin(\delta_1 t_1)+b\cos(\delta_1 t_1) +c\sin(3\delta_1 t_1)+d\cos(3\delta_1 t_1)\ . \tag{33}$$

This expression can be substituted into the reduced equation and the method of harmonic balance[17] applied to obtain approximate expressions for the coefficients. The desired correction coefficients for the fundamental sine and cosine terms are

$$a\approx(-1/\delta_1^3)[(\mu_1-3/4\delta_1^2)^2+1/16\delta_1^4]\ , \tag{34}$$

$$b\approx(1/\delta_1^2)(3/4\delta_1^2-\mu_1)\ . \tag{35}$$

b. $\mu_1>\mu_{1B}$. Here the solution is of the form

$$x_1(t)=K+\frac{1}{\delta_1}\sin(\delta_1 t_1)+f(t_1)\ , \tag{36}$$

where K is a constant and $f(t)$ is a small periodic function with zero time average. We would like an expression for K as a function of μ_1. Substituting the expression for x_1 into Eq. (18) for dx_1/dt_1 we find

$$df/dt_1\approx(\mu_1 K-K^3-3K/2\delta_1^2) +(\mu_1/\delta_1-3K^2/\delta_1)\sin(\delta_1 t_1) +(3K/2\delta_1^2)\cos(2\delta_1 t_1)-(1/\delta_1^3)\sin^3(\delta_1 t_1)\ , \tag{37}$$

where we have omitted all $f(t)$ terms on the right-hand side because the most significant of these terms is of the order of δ_1^{-6} while df/dt_1 is of the order of δ_1^{-3}. The solution to this equation cannot be periodic unless the constant term on the right-hand side is zero, hence

$$K\approx\pm(\mu_1-3/2\delta_1^2)^{1/2}\ . \tag{38}$$

Equation (37) is easily solved to obtain an approximation for the correction term $f(t_1)$ if desired.

IV. QUASISTATIC REGIME ($\delta/\epsilon^{2/3}\ll 1$)

A. Dynamical picture—occurrence of "square response"

We will start off this subsection by discussing the behavior of the first form of the rescaled equation, Eq. (18), in which ϵ has been suppressed, and then later we will discuss the second form, Eq. (20), in which μ has been suppressed.

In the limit $|\delta_1|\ll 1$, we can make the approximation that $\dot{x}_1\approx 0$ since the cosine term is changing very slowly. Thus the quasistatic equation is

$$\cos\phi=x_1^3-\mu_1 x_1\ , \tag{39}$$

where $\phi=\delta_1 t_1=\delta t$. This equation exhibits three different behavior patterns depending on the value of μ_1. The three cases are $\mu_1<0$, $0<\mu_1<\mu_{1B}$, and $\mu_1>\mu_{1B}$, where $\mu_{1B}=3/4^{1/3}\approx 1.889\,88$.

For $\mu_1<0$, the right-hand side of Eq. (39) is a monotonically increasing function of x_1. In this case there is a unique inverse to Eq. (39) giving x_1 as a continuous function of t, a typical case is shown in Fig. 2(a). At $\mu_1=0$, $x_1(t)$ develops two points of infinite slope as in Fig. 2(b). For $\mu_1>0$, the right-hand side of Eq. (39) is no longer monotonic, developing two extrema as shown in Fig. 3. There is now a central region in which there are three solutions for x_1 for a given value of $\cos(\delta_1 t_1)$. For $0<\mu_1<\mu_{1B}$, the extrema have magnitude less than 1. When the value of $\cos\phi$ passes one of these extremal points, a sudden transition takes place as shown in Fig. 3. This results in giving $x_1(\phi)$ a square-wave character as shown in Figs. 2(c) and 2(d). In particular, one has

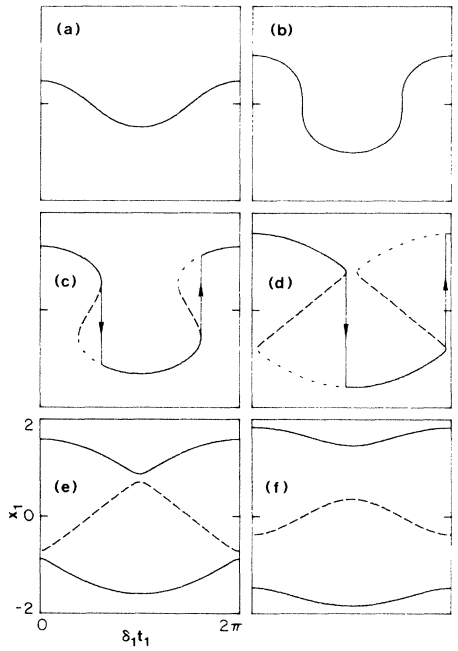

FIG. 2. Shows $x_1(t)$ for various values of the bifurcation parameter μ_1 in the quasistatic limit $|\delta_1|\ll 1$. Solid line, the attractor for $x_1(t)$. Dashed line, unstable solution to the quasistatic equation [Eq. (39)] for $x_1(t)$. Dotted line, other stable solution to Eq. (39) which is not part of an attractor. (a) $\mu_1=-\mu_{1B}$, where $\mu_{1B}\approx 1.889\,88$ is the shifted bifurcation point: $x_1(t)$ nearly a perfect cosine. (b) $\mu_1=0$: (original bifurcation point) nonlinearities become apparent. (c) $\mu_1=\frac{1}{2}\mu_{1B}$: transients occur, as in Fig. 3, giving $x_1(t)$ a square-wave character. (d) $\mu_1=0.99\mu_{1B}$ just below the shifted bifurcation point. (e) $\mu_1=1.01\mu_{1B}$ just above the shifted bifurcation point, transients no longer occur, two complementary attractors now exist, separated by an unstable orbit. (f) $\mu_1=\frac{3}{2}\mu_{1B}$, attractors now have little harmonic content.

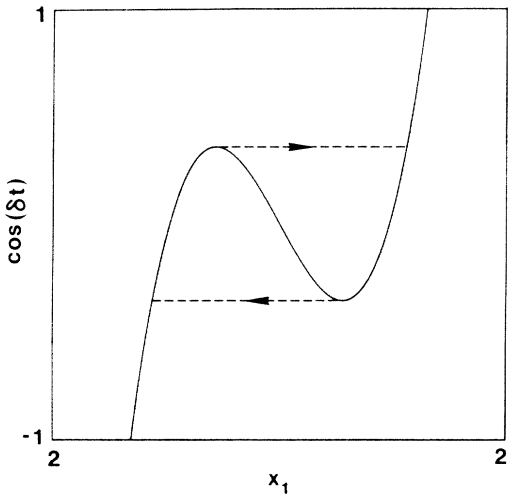

FIG. 3. Transients (dashed lines) occur when $\cos(\delta t)$ passes the extrema of $x_1^3-\mu_1 x_1$ in Eq. (39) giving $x_1(t)$ a square-wave character.

$$x_1(\phi)=\begin{cases}x_{1+}(\phi), & \phi_*<\phi<\phi_*+\pi\\ x_{1-}(\phi), & \phi_*+\pi<\phi<\phi_*+2\pi\end{cases}$$

$$x_1(\phi+2\pi)=x_1(\phi)\ ,$$

where x_{1+} is the most positive root of Eq. (39) and x_{1-} is the most negative root. The jumps occur at equally spaced intervals with the phase specified by the quantity

$$\phi_*=-\arccos(4\mu^3/27)^{1/2}\ ,$$

where ϕ_* is in the range $-\pi/2$ to 0. For $\mu_1>\mu_{1B}$ the extrema have magnitude greater than 1. Since this is out of range of the cosine function, the transitions no longer occur, and $x_1(\phi)$ is a continuous function again. However, $x_1(\phi)$ now has two stable solutions x_{1+} and x_{1-} which are complementary forms of each other, i.e., $x_{1+}(\phi)=-x_{1-}(\phi+\pi)$. These solutions are asymmetrical and have a constant component, as shown in Figs. 2(e) and 2(f). These two stable solutions are separated by a third solution, which is symmetrical but unstable. The appearance of the constant component in $x_1(\phi)$ results in the appearance of $\omega_0/2$ in the spectrum of $\mathbf{X}(t)$ as discussed in Sec. III E. However, this is not an ordinary period-doubling bifurcation in which there is a continuous change in $\mathbf{X}(t)$ with bifurcation parameter. Rather, in the $\delta_1\to 0$ limit, there is a discontinuous change in $x(\phi)$ [and therefore in $\mathbf{X}(t)$] at the bifurcation point as can be seen by comparing Figs. 2(d) and 2(e). This results in the sudden appearance of a response at $\omega_0/2$ of finite amplitude, and also a sudden drop in the response at ω_1, as is shown in detail in Sec. IV B. This discontinuity is an artifact of the quasistatic limit. However, for small detuning the true $x(t)$ exhibits an exceedingly abrupt (though continuous) change near the bifurcation point, which for all practical purposes may be considered a discontinuity and described by the quasistatic result. This is discussed further in Sec. V A.

So far we have been considering the behavior of Eq. (18) in which we have rescaled the parameters (ϵ, δ, and μ) so as to eliminate ϵ and assume it to be fixed. As we discussed in Sec. III C, we can eliminate μ instead, resulting in Eq. (20). This is useful for studying nonlinear gain effects, where ϵ is varied while μ is held fixed. The quasistatic form for this equation is

$$\epsilon_2\cos\phi=x_2^3-\mathrm{sgn}(\mu)x_2\ . \tag{40}$$

We are still considering the quasistatic case, but now the condition is that $|\delta_2|\ll 1$ (where $\delta_2=\delta/|\mu|$) rather than $|\delta_1|\ll 1$ (where $\delta_1=\delta/\epsilon^{2/3}$). There are clearly two forms of Eq. (40) depending on the sign of μ. For μ negative, the right-hand side of Eq. (40) is monotonic so there can be none of the switching behavior previously described. For small ϵ_2 the response $x_2(t)$ will be nearly sinusoidal with amplitude proportional to ϵ_2. For higher ϵ_2 the fundamental component of $x_2(t)$ will be reduced (from the linear gain result) due to the cubic nonlinearity. For μ positive the behavior is quite different: for sufficiently small ϵ_2 the system must be period doubled (i.e., have $\omega_0/2$ in its spectrum); but as ϵ_2 is increased, it reaches the critical value $\epsilon_{2B}=\mu_{1B}^{-3/2}=2/\sqrt{27}$, where $x_2(t)$ goes into the switching mode, and the period doubling is suppressed. This results in a dramatic and discontinuous change in the response, as will be seen in Sec. IV B. These nonlinear effects may have important practical ramifications for small-signal amplifiers. We return to this point in the final section.

B. System response at ω_1 and $\omega_0/2$

1. ϵ fixed, μ varied

Here we present the results of numerical studies of Eq. (18). The constant c_0 and fundamental c_1 Fourier components of $x_1(t)$ (as defined in Sec. III E) were determined for a large number of values of μ_1 in the range $-2\mu_{1B}$ to $+2\mu_{1B}$, where $\mu_{1B}=3/4^{1/3}$. There are two solutions for $x_1(t)$ in the period-doubled regime. We give data for the case with positive c_0; for the negative case multiply c_0 by -1 and leave c_1 unchanged.

The constant component c_0 is proportional to the amplitude of $\omega_0/2$ in the spectrum of the dynamical variable $\mathbf{X}(t)$ [related to $x(t)$ by Eq. (1)]. Below the shifted bifurcation point μ_{1B} the component c_0 is equal to zero. Crossing $\mu_1=\mu_{1B}$, it jumps discontinuously to a value $\alpha\equiv 4^{1/3}27^{1/2}/2\pi\approx 1.3128$ (the exact expression is derived in the Appendix). The results are shown graphically in Fig. 4(a). The solid line is the numerically determined value of c_0 for Eq. (39), while the dashed line gives the unperturbed behavior, i.e., Eq. (39) without the $\cos\phi$ term.

$|c_1|$ is proportional to the amplitude of ω_1 in the spectrum, and $|c_1|/c_0$ gives the ratio of the amplitudes of ω_1 and $\omega_0/2$. c_1 has both real and imaginary components corresponding to $\frac{1}{2}$ of the $\cos(\delta_1 t_1)$ and $-\frac{1}{2}$ of the $\sin(\delta_1 t_1)$ components of $x_1(t)$, respectively. These are plotted along with $|c_1|$ in Fig. 3(b). The $|c_1|$ curve was accurately followed by data taken in the analog simulations. These results are presented in Sec. VI. This curve is important to the theory of parametric amplifiers, as it describes how the gain at the signal (perturbation) frequency varies near the bifurcation point. As can be seen

in the figure, the gain continues to rise as we pass the original bifurcation point $\mu=0$. $|c_1|$ reaches a maximum value of approximately 0.897 609 at $\mu_1 \approx 1.779\,60$. It then decreases slightly to the value $\sqrt{7}\alpha/4$ ($\approx 0.868\,32$) at $\mu_1=\mu_{1B}\approx 1.889\,88$. At this point there is a discontinuous drop in $|c_1|$ to $\alpha/8$ ($\approx 0.164\,10$), followed by further decrease as μ increases. The exact values of c_1 on both sides of the discontinuity are calculated in the Appendix.

The value of $\mathrm{Im}c_1$ can be determined exactly for all values of μ_1. It is zero except in the interval $0<\mu_1<\mu_{1B}$ where the hysteretic transitions in the cycle (see Fig. 3) break the cosine symmetry allowing a sine component. The integral in ϕ defining $\mathrm{Im}c_1$ can be converted to a simple integral in x yielding

$$\mathrm{Im}c_1 = -3\mu_1^2/4\pi \ . \tag{41}$$

2. μ fixed, ϵ varied

As pointed out in Sec. III C there are transformations between the variables and parameters of the ϵ-fixed (subscript 1) case and those of the μ-fixed (subscript 2) case. Here we need $\epsilon_2 = |\mu_1|^{-3/2}$ and $x_2 = x_1/|\mu_1|^{1/2}$. Since this case has some very interesting features, we have converted the numerical results plotted in Fig. 4 and present them in Fig. 5. (Note that here c_0 and c_1 are components of x_2, not x_1.)

For $\mu<0$ [Fig. 5(a)] the behavior is linear for small ϵ, but the gain falls off for higher ϵ, with c_1 eventually going like $\epsilon_2^{1/3}$ for large ϵ_2. c_0 is always zero in this case.

For $\mu>0$ [Figs. 5(b) and 5(c)] something much more interesting occurs: the c_0 and $|c_1|$ components of $x_2(t)$ have very pronounced step-function-like behavior. This step occurs at $\epsilon_2=\epsilon_{2B}=2/27^{1/2}$, as discussed in Sec. IV A. This behavior occurs to all higher harmonics c_n of $x(t)$ as well: the even-n components switch off, while the odd ones undergo a dramatic increase. (Note that at the bifurcation point the behavior of all the c_n may be determined exactly; see Secs. 2 and 3 of the Appendix.) This type of behavior could be very useful in producing a switchlike response to a perturbation signal when it crosses the critical amplitude threshold.

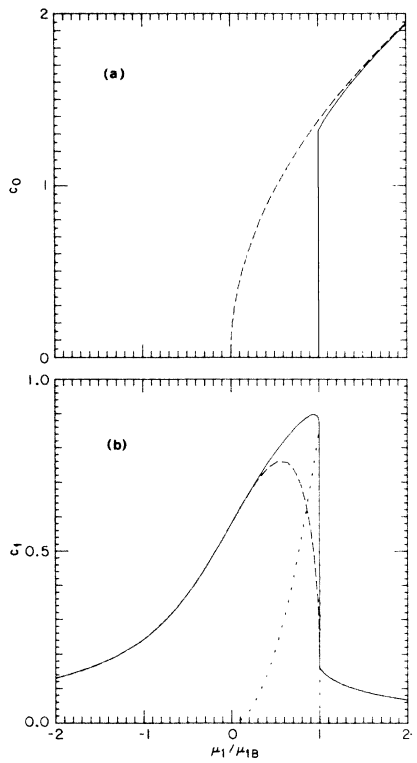

FIG. 4. Numerical determination of constant, c_0, and fundamental, c_1, components of $x_1(t)$ for $|\delta_1| \ll 1$. These are proportional to the $\omega_0/2$ and ω_1 components of the dynamical variable $\mathbf{X}(t)$, respectively. (a) Solid line: c_0 as a function of parameter μ_1. Note that $c_0=0$ for $\mu_1<\mu_{1B}$. Dashed line: unperturbed result, goes as $\mu_1^{1/2}$. (b) Solid line: $|c_1|$ as a function of parameter μ_1. Dashed line: $\mathrm{Re}c_1$, this is $\frac{1}{2}$ the $\cos(\delta t)$ component of $x_1(t)$. Dotted line: $-\mathrm{Im}c_1$, this is $\frac{1}{2}$ the $\sin(\delta t)$ component of $x_1(t)$.

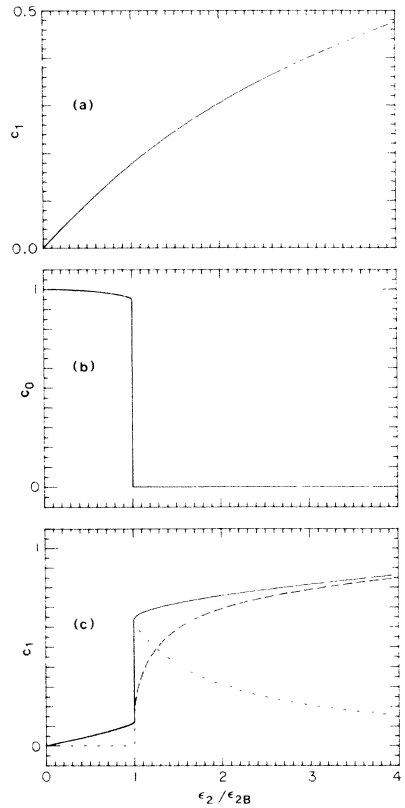

FIG. 5. Nonlinear gain behavior; perturbation amplitude ϵ varied while μ held fixed, numerically determined in the quasistatic limit, Eq. (40). (a) $\mu<0$ case, gives fundamental component c_1 (real) as a function of ϵ_2/ϵ_{2B}, where $\epsilon_{2B}=2/27^{1/2}$. Shows how gain falls off at high amplitude. (b) $\mu>0$ case, shows c_0, the constant component of the reduced variable (corresponding to the $\frac{1}{2}\omega_0$ component of the dynamical variable) which switches off for $\epsilon_2>\epsilon_{2B}$. (c) $\mu>0$ case, shows c_1, the fundamental component of the reduced variable (corresponding to the ω_1 component of the dynamical variable), which is also discontinuous at $\epsilon_2=\epsilon_{2B}$. Solid line, $|c_1|$; dashed line, $\mathrm{Re}c_1$, dotted line, $-\mathrm{Im}c_1$.

3. Asymptotic behavior

In Secs. IV B 1 and IV B 2 numerical results were presented showing how the response at frequencies ω_1 and $\omega_0/2$ varied with bifurcation parameter and perturbation amplitude in the nonlinear region where x^3 and μx are comparable in magnitude. Considerable simplification results in the limit of large μ or small ϵ. The results can be applied to the behaviors of both of the rescaled equations, i.e., Eqs. (39) and (40).

The asymptotic behavior of c_1 in the limit $\mu/\epsilon^{2/3}\rightarrow-\infty$ may be determined directly from the asymptotic form of $x(t)$, i.e., Eq. (28) of Sec. III F. In the $\delta\rightarrow 0$ limit this becomes

$$x(t)=-(\epsilon/\mu)\cos(\delta t) . \tag{42}$$

It immediately follows that

$$\lim_{\mu/\epsilon^{2/3}\rightarrow-\infty} c_1=-\epsilon/2\mu . \tag{43}$$

Here c_1 is the fundamental Fourier component of $x(t)$. The result is easily converted for the rescaled cases: for $x_1(t)$, $c_1=-1/2\mu_1$, and for $x_2(t)$, $c_1=-\epsilon_2/2$.

Since c_1 is proportional to ϵ, it is clear that the system will behave like a linear amplifier, producing a response at the perturbation frequency, ω_1, which is proportional to the amplitude of the perturbation. The result can be used to extend the range of Fig. 4, as it is already a good approximation at $\mu_1=-2\mu_{1B}$.

In the $\mu/\epsilon^{2/3}\rightarrow+\infty$ limit, the asymptotic behavior is determined by Eq. (31). In the $\delta\rightarrow 0$ limit this becomes

$$x(t)=\mu^{1/2}+(\epsilon/2\mu)\cos(\delta t) . \tag{44}$$

Thus we find

$$\lim_{\mu/\epsilon^{2/3}\rightarrow+\infty} c_0=\mu^{1/2} , \tag{45}$$

$$\lim_{\mu/\epsilon^{2/3}\rightarrow+\infty} c_1=\epsilon/4\mu . \tag{46}$$

Again, these are Fourier components of $x(t)$; for $x_1(t)$, $c_0=\mu_1^{1/2}$ and $c_1=1/4\mu_1$; for $X_2(t)$, $c_0=1$ and $c_1=\epsilon_2/4$. Note that the asymptotic behavior of c_1 is not symmetric about $\mu=0$, going like $\epsilon/2|\mu|$ for the $\mu<0$ case and $\epsilon/4|\mu|$ for the $\mu>0$ case. Like the previous case, these results can be used to extend the range of Fig. 4; they are already good approximations at $\mu_1=+2\mu_{1B}$.

To extend the range of Fig. 5, we need the behavior for large ϵ_2. This corresponds to small μ_1 in Fig. 4. For small μ_1, we expand c_1 in a power series in μ_1:

$$c_1=K_0+K_1\mu_1+\cdots . \tag{47}$$

Here we will only evaluate K_0 and K_1. From Eq. (39) we find

$$\partial x_1/\partial\mu_1=x_1/(3x_1^2-\mu_1) . \tag{48}$$

For μ_1 small this is approximately $1/3x_1$. Using the fact that $x_1=\cos^{1/3}\phi$ at $\mu_1=0$, we expand x_1 for small μ_1 as

$$x_1\approx\cos^{1/3}\phi+\mu_1/(3\cos^{1/3}\phi) . \tag{49}$$

From this we obtain an approximation for c_1:

$$\lim_{\mu_1\rightarrow 0} c_1=(1/2\pi)\int_0^{2\pi}[\cos^{4/3}\phi+(\mu_1/3)\cos^{2/3}\phi]d\phi . \tag{50}$$

This integral can be done (use 3.621-1 from Ref. 19) resulting in

$$\begin{aligned} K_0&=3\Gamma(\tfrac{1}{3})^3/(\pi^2\times 2^{10/3})\approx 0.579\,797\,3 ,\\ K_1&=2^{4/3}\pi/[3^{1/2}\times\Gamma(\tfrac{1}{3})^3]\approx 0.237\,724\,7 . \end{aligned} \tag{51}$$

The result is easily transformed to the second form equation for x_2 in terms of ϵ_2:

$$c_1=K_0\epsilon_2^{1/3}+K_1\mathrm{sgn}(\mu)\epsilon_2^{-1/3} . \tag{52}$$

This extends the results given graphically in Figs. 5(a) and 5(c) to higher values of ϵ_2. Its accuracy is about 1% at the maximum values graphed and improves for higher ϵ_2.

V. DYNAMIC REGIME

This section deals with the behavior of the reduced equation when the detuning is significant. Unlike the previous section we will work solely with the first rescaled form of the equation, Eq. (18).

A. Crossover to ordinary period doubling

From the discussion of the quasistatic case, it should be clear that a degenerate sort of period-doubling bifurcation occurs in the $\delta_1\rightarrow 0$ limit. In that case the reduced variable $x_1(t)$ makes a discontinuous (but nonhysteretic) change as μ_1 passes the bifurcation point. In this section, we show that for small (but nonzero) δ_1 an ordinary period-doubling bifurcation does take place, but very rapidly over a small interval of μ_1. Figure 6 shows a sequence of events occurring in the case of $\delta_1=0.1$. This sequence shows how $x_1(t)$ evolves from the switchlike behavior expected below μ_{1B} to the continuous but asymmetrical behavior expected above μ_{1B}. What happens is that for μ_1 just slightly below the quasistatic value of μ_{1B} $(=3/4^{1/3})$, the orbit will (for very carefully chosen μ_1) tend to delay its transitional jump of the quasistatic picture and go part way down the unstable (negative slope) section of $x_1^3-\mu_1 x_1$ as shown in Fig. 6(a). Such an orbit can be stable as long as the time integral of $\mu_1-3x_1^2$ $(=d\dot{x}/dx)$ over the *whole orbit* is negative. As μ is increased, the orbit extends farther down the unstable branch until it finally loses stability in a symmetry-breaking bifurcation, Fig. 6(b), at $\mu=\mu_{1B}$ (note that μ_{1B} depends on μ_1). Beyond this point there are two asymmetrical attractors which are inverse images of each other. Initially the two attractors include both positive and negative values of x_1 [Figs. 6(c) and 6(d)], but they eventually separate at $\mu=\mu_{1S}$ [Fig. 6(e)], $x_{1+}(t)$ being entirely positive and $x_{1-}(t)$ being entirely negative. Beyond this point the portion of the orbit in the unstable (negative slope) section of $x_1-\mu_1 x_1$ rapidly decreases as shown in Fig. 6(f). The change in μ_1 between Figs. 6(b) and 6(e) is exceedingly small, approximately 5.293×10^{-11}. This is called the bifurcation width and is discussed further in

Sec. V C. Note that in going from Fig. 6(c) to 6(d) one of the "lobes" of the attractor diminishes in size and vanishes. This occurs over an extremely short interval of μ_1, even compared to the bifurcation width.

B. Bifurcation shift versus detuning

1. Numerical results

The shifted bifurcation point μ_{1B} is a function of the rescaled detuning δ_1 ($\delta_1=\delta/\epsilon^{2/3}$). At $\mu_1=\mu_{1B}$ there is a symmetry-breaking bifurcation of the reduced variable $x_1(t)$ which corresponds to the period-doubling bifurcation of the dynamical variable $\mathbf{X}(t)$. By numerically studying the attractor for Eq. (18) and looking for the point where asymmetry commences or by studying the stability integral ($\int \mu - 3x^2 dt$) one can accurately determine μ_{1B} as a function of δ_1. This function is plotted in Fig. 7. Perhaps the most striking feature of this figure is the pointed peak, at which point the derivative is discontinuous. We were able to accurately reproduce this curve including the pointed peak with data taken in the analog simulation of Duffing's equation (Sec. VI).

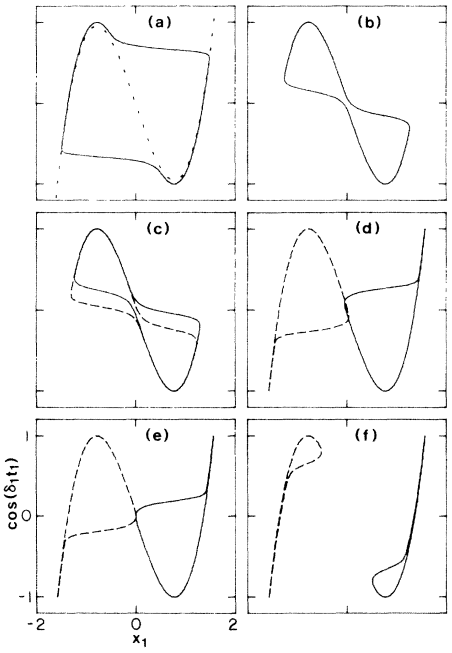

FIG. 6. Sequence shows the behavior of $x_1(t_1)$ very near the bifurcation point μ_{1B} ($\approx 1.831\,322\,477\,570\,70$) for a detuning of $\delta_1=0.1$. Solid line shows the attracting solution $x_1(t_1)$ vs $\cos(\delta_1 t_1)$. Dotted line [(a) only] shows the function $x_1^3-\mu_1 x_1$ which the attractor follows (in the $\delta_1\to 0$ limit) except during transient jumps. Dashed line shows the complementary attractor which exists for the cases beyond the bifurcation point [(c)–(f)]. (a) $\mu_1=0.999\mu_{1B}$. (b) $\mu_1=\mu_{1B}$, the bifurcation point. (c) $\mu_1=\mu_{1B}+\frac{1}{3}\mu_{1W}$, where $\mu_{1W}=5.293\times 10^{-11}$. (d) $\mu_1=\mu_{1B}+\frac{2}{3}\mu_{1W}$. (e) $\mu_1=\mu_{1B}+\mu_{1W}\equiv\mu_{1S}$, the separation point. (f) $\mu_1=1.001\mu_{1B}$.

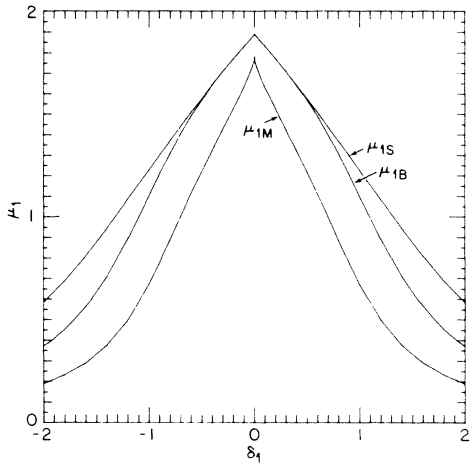

FIG. 7. Numerical results for Eq. (18) showing three functions of the rescaled detuning μ_1: μ_{1B} the bifurcation point, μ_{1M} the maximum gain point, and μ_{1S} the separation point. For $|\delta_1|>2$, asymptotic formulas may be used which are given in the text.

2. Small-δ_1 limit

It is possible to determine the slope $d\mu_{1B}/d\delta_1$ exactly in the limit $\delta_1\to 0$. We present here a heuristic argument which has been checked numerically to reasonable accuracy. The approach is to use the fact that $\cos(\delta_1 t_1)$ and $x_1^3-\mu_1 x_1$ both exhibit quadratic extrema. We will discuss the behavior near the maximum of $\cos(\delta_1 t_1)$, occurring at $t_1=0$, and the maximum of $x_1^3-\mu_1 x_1$ occurring at $x_1=-(\mu_1/3)^{1/2}$. The behavior at the corresponding minima is related by symmetry.

In the quasistatic picture, a sudden transition occurs when $\cos(\delta_1 t_1)$ increases past this maximal value of $x_1^3-\mu_1 x_1$. However, as discussed in Sec. V A, when μ_1 is very near the bifurcation point μ_{1B}, this transition is delayed, and the cosine function tends to follow $x_1^3-\mu_1 x_1$ into the unstable negative slope region. Thus the quadratic maxima of $\cos(\delta t)$ and $x_1^3-\mu_1 x_1$ must nearly coincide, i.e., $x_1\approx -(\mu_1/3)^{1/2}$ at $t=0$. Expanding $x_1^3-\mu_1 x_1$ and $\cos(\delta_1 t_1)$ through quadratic terms about their maxima, Eq. (18) becomes

$$\dot{x}_1 \approx 1-2(\mu_1/3)^{3/2}+3(\mu_1/3)^{1/2}[x_1-(\mu_1/3)^{1/2}]^2 - \delta_1^2 t_1^2/2 \ . \tag{53}$$

This equation has one very simple solution, which exists only for certain values of μ_1 and δ_1. The solution is

$$x_1=-(\mu_1/3)^{1/2}+[1-2(\mu_1/3)^{2/3}]t_1 \tag{54}$$

and it has the property that $\dot{x}$ is constant. It is easily verified that this occurs when μ_1 and δ_1 are related by

$$\delta_1=\pm(12\mu_1)^{1/4}[1-2(\mu_1/3)^{3/2}] \ . \tag{55}$$

This solution has the important property that $\dot{x}$ is small for negative t and remains small for positive t in the unstable region of x_1. This indicates that the system is very near the bifurcation point since the switching behavior which normally occurs upon reaching the unstable region

has been suppressed. Differentiating Eq. (55) one obtains a linear approximation for the bifurcation point μ_{1B} as a function of δ_1:

$$\mu_{1B} \approx 3/4^{1/3} - (1/3^{1/2})\,|\,\delta_1\,|\ . \tag{56}$$

Numerical results agree with the linear expression given above for small δ_1; however, higher-order terms determined numerically do not agree with those implied by Eq. (55). Apparently, the approximations we made are not valid beyond the linear term.

3. *Asymptotic behavior, $\delta_1 \to \infty$*

In the period-doubled regime, we obtained [Eq. (36)] the asymptotic expression $x_1(t_1) \approx K + (1/\delta_1)\sin(\delta_1 t_1)$, where K is approximately $(\mu_1 - 3/2\delta_1^2)^{1/2}$. The presence of the constant K in the solution for the reduced variable $x_1(t)$ corresponds to the presence of $\omega_0/2$ (i.e., period doubling) in the spectrum of the dynamical variable $\mathbf{X}(t)$. Thus the bifurcation point (where K vanishes) is

$$\lim_{\delta_1 \to \infty} \mu_{1B} = 3/2\delta_1^2\ . \tag{57}$$

This result has been checked numerically at $\delta_1 = 2$ where $\mu_{1B} = 0.371\,135$, a 1% deviation from the formula, and at $\delta_1 = 10$ where $\mu_{1B} = 0.014\,999\,989\,8$, a 0.0001% deviation.

C. Bifurcation width

As discussed in Sec. V A, near the bifurcation point, $x(t)$ changes very rapidly over a very small parameter interval (relative to the bifurcation shift) when the detuning is small. In order to obtain a measure of this interval and how it varies with detuning, we define the separation point μ_{1S}. This is the point following the bifurcation at which the two attractors no longer overlap, $x_{1+}(t)$ being entirely positive and $x_{1-}(t)$ being entirely negative, as shown in Fig. 6(e). The bifurcation width μ_{1W} is just the difference between the separation point and the bifurcation point.

The separation point is actually quite easy to observe experimentally, provided the detuning is not too small. As discussed in Sec. III B, the dynamics of the reduced variable $x(t)$ are related to the behavior of the Poincaré map. Beyond the bifurcation point, the iteration sequence in the Poincaré section goes back and forth between points contained in two line segments. These segments are constrained to be collinear and initially overlap. μ_{1S} is the point beyond which they no longer do so.

In Fig. 7 we show numerical results giving the separation point as a function of detuning for Eq. (18). As can be seen, the bifurcation width is extremely small below a detuning of about 0.6.

Numerical results indicate that the bifurcation width falls off very rapidly with δ_1. The smallest value measured was at $\delta_1 = 0.1$ where $\mu_{1W} \approx 5.293 \times 10^{-11}$. This is certainly far beyond the resolution of most experiments. Thus the discontinuities of the quasistatic picture will effectively be observed in real experiments with finite detuning. The reason for the rapid decline in width is that, as discussed in Sec. V A, when one is near the bifurcation point, the orbit must spend about half its time in the unstable region of x_1, where $x_1^3 - \mu_1 x_1$ has negative slope. Deviations from the correct orbit in the unstable region grow exponentially. This sensitivity goes like e^{1/δ_1}, since a decrease in δ_1 increases the time spent in the unstable region during each cycle. An approximate empirical fit to the numerical data is

$$\mu_{1W} \approx 1.132\delta_1^{1.22}\exp(-2.0977/\delta_1)\ . \tag{58}$$

This is accurate to about 2% over the range $0.1 < \delta < 0.75$ which corresponds to $5 \times 10^{-11} < \mu_{1W} < 5 \times 10^{-2}$.

The asymptotic form of $x_1(t)$ is studied in Sec. III F 3 b, and found to be

$$x_{1+}(t) \approx (\mu_1 - 3/2\delta_1^2)^{1/2} + (1/\delta_1)\sin(\delta_1 t_1)$$

[see Eqs. (36) and (38)]. This solution will be entirely positive when $(\mu_1 - 3/2\delta_1^2)^{1/2} = 1/\delta_1$, hence the asymptotic behavior of μ_{1S} is

$$\lim_{\delta_1 \to \infty} \mu_{1S} = 5/2\delta_1^2\ . \tag{59}$$

This formula was checked numerically at $\delta_1 = 10$. Here $\mu_{1S} = 0.025 \pm 5 \times 10^{-6}$, so the deviation from the formula at this point is less than 0.02%.

D. Maximum gain versus detuning

We saw in the quasistatic case that the maximum gain (or response at ω_1) occurs slightly below the shifted bifurcation point. This type of behavior continues into the region where δ_1 is significant, i.e., the maximum gain lies between $\mu_1 = 0$ and $\mu_1 = \mu_{1B}$. We will call the maximum gain point μ_{1M} and the value of the fundamental Fourier component at this point c_{1M}. In Fig. 7 we plot the numerical results for μ_{1M} versus δ_1 and in Fig. 8 we plot c_{1M} versus δ_1. Note the interesting cusps that occur at $\delta_1 = 0$.

In Sec. III F we showed that in the $\delta_1 \to \infty$ limit, $x_1(t)$

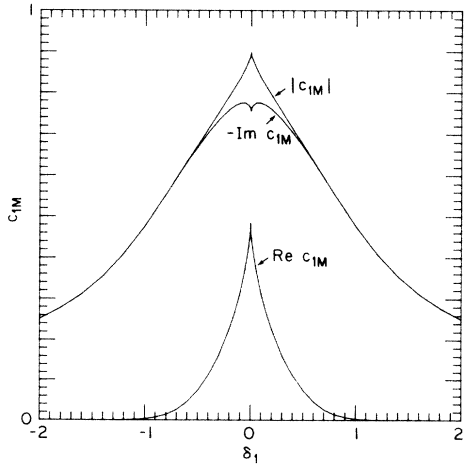

FIG. 8. Plots of c_{1M} vs δ_1 where c_{1M} is the value of the fundamental Fourier component of $x_1(t)$ at the maximum gain point μ_{1M} (see Fig. 7). This corresponds to the maximum obtainable response at the perturbation frequency for a particular detuning and perturbation amplitude.

can be approximated by Eq. (33). We are interested in the expressions for the coefficients a and b [Eqs. (34) and (35)] of the sine and cosine components, respectively. In terms of a and b, $|c_1|$ (the fundamental Fourier component) is

$$|c_1| = \tfrac{1}{2}[(a+1/\delta_1)^2+b^2]^{1/2}$$
$$\approx 1/2\delta_1 - 1/32\delta_1^6 - (1/4\delta_1^2)(\mu_1 - 3/4\delta_1^2)^2 . \quad (60)$$

From this expression, we find that asymptotically the maximum occurs at

$$\lim_{\delta_1 \to \infty} \mu_{1M} \approx 3/4\delta_1^2$$

and has amplitude

$$c_{1M} \approx (-i)(1/2\delta_1 - 1/32\delta_1^6) . \quad (61)$$

VI. ANALOG SIMULATIONS

A. Description of the simulator

In order to get some idea how well the theoretical results might be followed by a specific physical system, we chose to study the forced Duffing's equation on an analog simulator. The perturbation term $E\cos(\omega_1 t)$ is added to the forcing term resulting in the equation

$$\ddot{y} + \gamma\dot{y} + \alpha y + \beta y^3 = A + B\cos(\omega_0 t) + E\cos(\omega_1 t) . \quad (62)$$

The simulator is a precision electronic circuit whose primary components are two integrators (to convert $\ddot{y}$ into y) and two multipliers (to produce y^3 from y). This system was adjusted to the threshold of a period-doubling bifurcation at the approximate parameter setting: $\gamma \approx 6.7\times 10^2$, $\alpha \approx 1.5\times 10^5$, $\beta \approx 3.0\times 10^4$, $A \approx 3.5\times 10^6$, $B \approx 2.4\times 10^6$, and $\omega_0 \approx 2\pi \times 502$ Hz. In the form of the equation above, y was measured directly from an output of the simulator in volts, and $\omega_0/2\pi$ is the frequency of the forcing oscillator in hertz. Typical oscillations were on the order of 10 V in amplitude. Note that the equation can be simplified, if desired, by rescaling y and t so as to set two of the parameters (such as α and β) to unity. The constant forcing term A was produced by applying a voltage reference V_{dc} to the system [where $A = (3\times 10^6)V_{dc}$]. This term is very important in that it breaks the symmetry of the equation, which in turn makes it easier for the system to reach a period-doubling bifurcation (without the prerequisite of a symmetry-breaking bifurcation as in a symmetric system). ΔV_{dc} was used as our bifurcation parameter, where ΔV_{dc} is V_{dc} minus the bifurcation value of V_{dc} (~ 1.17 V). Note that in some of our data we give the measured perturbation amplitude as V_{sig}, where $E = (4.24\times 10^5)V_{sig}$.

In using a simulator, as in experimental systems, one has to consider the effects of noise. Consequently it is necessary to compromise between using low-amplitude signals, where noise interferes, and high-amplitude signals, where higher-order nonlinearities will affect the quantitative agreement with the theory. Several of the results we present were done for $V_{sig} = 80$ mV, at which point the response of the system to this perturbation can be on the order of 5–10% of the amplitude of the fundamental oscillation. As the reader will see in the following sections, we obtained very good agreement with the theory.

B. Rescaling experimental data

In our simulations (or any similar experiment), we are concerned with three types of parameters. (1) Detuning—in our experiment there is a driver (or pump) at frequency ω_0 and a perturbation (or signal) at frequency ω_1. We vary the detuning by changing ω_1 and define it as $\delta = \omega_1 - \omega_0/2$. (2) Perturbation amplitude—we control the amplitude V_{sig} [$\propto E$ in Eq. (62)], and we assume that ϵ (from the theory) is proportional to V_{sig}. (3) Bifurcation parameter—we varied this by adjusting ΔV_{dc} [$V_{dc} \propto A$ in Eq. (62)], but other parameters could have been used instead. We assume $\mu \propto \Delta V_{dc}$, i.e., higher-order corrections are neglected. In order to compare our results with the theory, V_{sig} and ΔV_{dc} must be rescaled to obtain ϵ and μ. However, most of the numerical results are given in terms of μ_1 and δ_1, where $\mu_1 = \mu/\epsilon^{2/3}$ and $\delta_1 = \delta/\epsilon^{2/3}$. By rescaling an appropriate theoretical curve to match (as closely as possible) the experimental data, we can calculate ϵ/V_{sig} and $\mu/\Delta V_{dc}$. In addition there is a scale factor relating the amplitudes of measured spectral components at frequencies $\omega_0/2 + m\delta$ to the Fourier components $|c_m|$ of $x_1(t)$ as determined by the theory.

C. Data compared to theory

Here we present the results of our analog simulations. A very simple but striking result is a plot of bifurcation shift versus perturbation amplitude for small detuning. This is shown in Fig. 9, a log-log plot constructed to demonstrate the $\frac{2}{3}$ power law. The solid line is drawn through the lowest amplitude point with a slope of $\frac{2}{3}$. As can be seen, it is almost a perfect fit over the range shown, over which the perturbation amplitude was increased by a

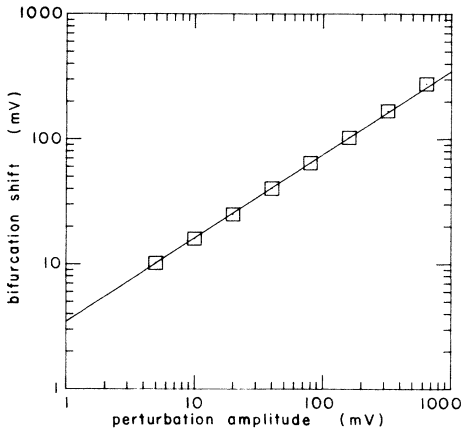

FIG. 9. Data from the simulator, showing the bifurcation shift ΔV_{dc} plotted against the perturbation amplitude V_{sig} on a log-log scale. The data are for very small detuning. This demonstrates the $\frac{2}{3}$ power law. The solid line has slope exactly $\frac{2}{3}$ and passes through the lowest amplitude point.

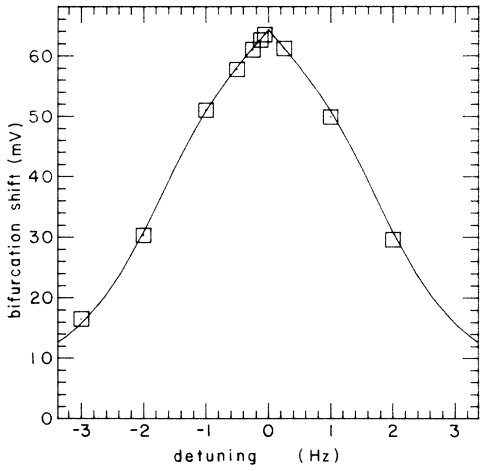

FIG. 10. Bifurcation shift ΔV_{dc} as a function of detuning δ. Rescaled for best fit to theoretical curve (solid line) from Fig. 6. Note that the simulation data points follow the pointed peak of the theoretical curve.

factor of 128. The detuning was decreased as low as could reasonably be achieved, approximately 0.03 Hz.

Another impressive result is a plot of bifurcation shift versus detuning for a constant perturbation amplitude, shown in Fig. 10. The distinctive "pointed peak" predicted by the theory (Sec. V B) is accurately followed by the data. The solid line is the theoretical curve (generated numerically) and the scaling factors for the experimental data were determined so as to obtain the best fit to this curve.

In Fig. 11 we show the response of the system at the perturbation frequency as a function of bifurcation parameter, for very small detuning—approximately 0.10 Hz. This shows what is perhaps the most dramatic effect: the discontinuity at the shifted bifurcation point. As discussed in Sec. V, while the discontinuity only really exists in the limit of $\delta \to 0$, it exists for all practical purposes for

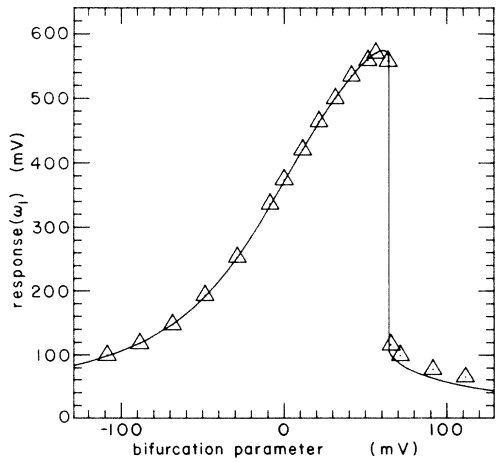

FIG. 11. Amplitude of the ω_1 spectral component of $y(t)$ from the simulator [response (ω_1)] vs bifurcation parameter (ΔV_{dc}). Theoretical curve (solid line) rescaled for best fit to data points. Perturbation amplitude $V_{sig}=80$ mV, detuning very small, approximately 0.1 Hz.

small but nonzero δ. The slope becomes exceedingly steep with decreasing δ—at $\frac{1}{10}$ Hz for the results just given, this slope is theoretically on the order of 10^{17} [see Eq. (58)]. As can be seen, the data in Fig. 11 fit the theoretical (solid line) results very well, especially below the shifted bifurcation point. The slight upward offset of the last four points is possibly a measurement error due to the close proximity of the large $\frac{1}{2}\omega_0$ peak to the much smaller ω_1 peak being measured.

Our final result, Fig. 12, shows the spectrum for three different cases of the bifurcation parameter. These cover the range $\frac{1}{2}\omega_0-20\delta$ to $\frac{1}{2}\omega_0+20\delta$, with δ set to approximately 0.120 Hz, and $\frac{1}{2}\omega_0=251$ Hz. The three cases correspond to the three cases studied theoretically in the Appendix: (a) $\mu_1=0$, the unperturbed bifurcation point; (b) $\mu=\mu_{1B-}$, just before the shifted bifurcation (as close as stability will allow); and (c) $\mu_1=\mu_{1B+}$, just after the shifted bifurcation point. These spectra measure the frequency components of $y(t)$, the Duffing variable of Eq. (62), and were measured with a Hewlett Packard Model 3582A spectrum analyzer connected to the Duffing simulator. The agreement of these three cases with theory is quite

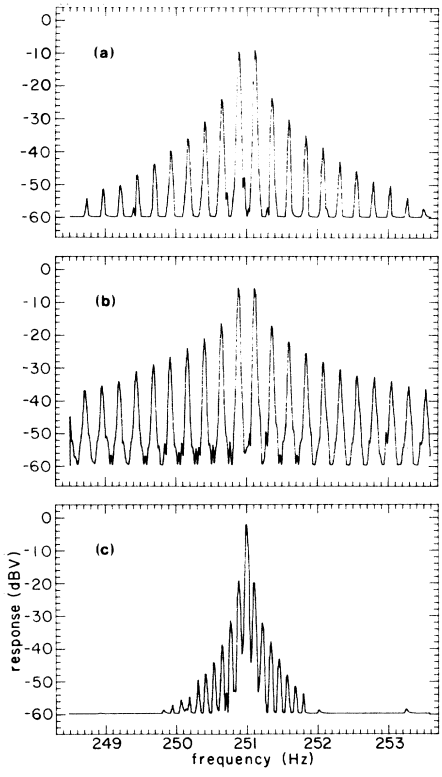

FIG. 12. Spectra (spectral peaks near $\omega_0/2$) for three values of bifurcation parameter. Response given in dB V which is $20\log_{10}$ of the rms amplitude in volts. All at $V_{sig}=80$ mV. Peaks appear at $\omega_{nm}=n(\omega_0/2)+m\delta$, where $\omega_0=2\pi\times 502$ Hz, and $\delta=2\pi\times 0.12$ Hz. Cases shown are for $n=1$ (n must be odd). (a) $\Delta V_{dc}=0$, unperturbed bifurcation point. Only odd-m peaks appear. (b) $\Delta V_{dc}=63.2$ mV just before the shifted bifurcation point of 63.4 mV. Note the lower fall-off rate of the peaks compared to (a). (c) $\Delta V_{dc}=64.9$ mV just after the shifted bifurcation point. Even-m peaks appear, but fall-off rate much greater than (a) or (b).

good, although the experimental peaks show a slightly greater fall-off rate in amplitude, presumably because of the nonzero detuning.

These three cases of the spectrum are probably the only ones for which the complete spectrum may be expressed in terms of standard functions as shown in the Appendix. They help to illustrate the changes which occur in the spectrum as μ passes the old and new bifurcation points. Below $\mu=0$, the peaks fall off rapidly with increasing n, faster than any power law as $n\to\infty$. For $\mu\ll 0$ only the two central peaks (ω_1 and $\omega_0-\omega_1$) are significant. At $\mu=0$ the peaks fall off less rapidly but still faster than $1/n$ (one can show that they fall off like $n^{-4/3}$). For $0<\mu_1<\mu_{1B}$ the emerging square-wave character of $x_1(t)$ results in an amplitude fall off that goes like $1/n$ (thus power falls off like $1/n^2$). At $\mu_1=\mu_{1B+}$ there is a sudden increase in the amplitude fall-off rate to $1/n^2$, combined with the sudden appearance of the even n peaks. For $\mu_1>\mu_{1B}$ the peaks fall off very rapidly as in the $\mu_1<0$ case. Finally, for $\mu_1\gg\mu_{1B}$ the central $\omega_0/2$ peak is much greater than all others.

VII. DISCUSSION AND CONCLUSIONS

We have detailed a variety of phenomena that occur when dynamical systems near the onset of a period-doubling bifurcation are subject to near-resonant perturbations. Our results are based on an analysis of the first-order nonlinear differential equation (2) governing the *scalar* function $x(t)$, which is related to the full *vector* dynamical variable $\mathbf{X}(t)$ via Eq. (1). Regardless of the precise evolution equations governing $\mathbf{X}$, it is the first-order equation (2) that captures the important behavior in the vicinity of the bifurcation point.

That the behavior of even high-dimensional systems may be deduced from a study of a much lower-dimensional equation is a familiar notion in the field of bifurcation theory.[15,20] This reduction of dimension follows rigorously near the onset of a bifurcation by an application of the center manifold theorem. Although we have not performed a mathematically rigorous reduction via the center manifold theorem to obtain our "normal form" Eq. (2), we have seen nevertheless that the reduced equation allows us to understand in great detail the effect of near-resonant perturbations. Moreover, our analysis goes far beyond the linearized theory previously developed,[1,2] which works well provided the perturbation is sufficiently small. In this paper, we have demonstrated that one can understand a host of phenomena that arise when the perturbations are somewhat larger by including a nonlinear term in the normal form.

Of all our results, perhaps the most interesting is that near-resonant perturbations *always*[21] suppress the onset of subharmonic oscillations—in this sense, one may say that the modulations serve to *stabilize* the dynamical system. This behavior has been verified in our analog simulations of the Duffing equation for a variety of parameter values and also in observations of the forced magnetic oscillator. We emphasize that the generality of this result does not depend on the perturbation being purely sinusoidal; however, one crucial property of the perturbation is that its time-average is zero. To see why this last condition is necessary, consider again the Duffing equation (62): if the perturbation had a nonzero time average, this constant offset could be absorbed into the parameter A. By simply changing the sign of this offset, one could either push the system out of, or drive it into, the period-doubled regime. (An entirely analogous conclusion was reached in the work on parametric forcing of a one-dimensional oscillator near the onset of a fixed-point pitchfork bifurcation, mentioned in the Introduction.[11])

The idea that near-resonant perturbations suppress the onset of subharmonic oscillations might strike some people as counter-intuitive. After all, if the unperturbed system is close to the period-doubling bifurcation point, one expects the system to be "soft" to modulations at the incipient frequency. However, one must remember that our analysis considers specifically the case where the unperturbed system is externally driven (i.e., nonautonomous): for example, in our simulations of the Duffing equation, Eq. (62), the driving terms $B\cos(\omega_0 t)$ and $E\cos(\omega_1 t)$ represent inputs from two distinct signal generators. On the other hand, if the unperturbed system were autonomous, then a large enough perturbation can cause *frequency locking* (also called entrainment) wherein the unperturbed oscillation frequency shifts to twice the perturbation frequency. We expect that frequency locking should occur more readily—that is, for decreasing perturbation amplitude ϵ—as either the detuning δ decreases, or as the bifurcation parameter μ tends toward μ_B. While the occurrence of frequency locking is bound to be an important ingredient in understanding the behavior of autonomous systems subject to near-resonant perturbations, in the case analyzed in the present paper this additional complication is not present.

As mentioned in the Introduction, an important motivation for this work has been a recently proposed small-signal amplification theory for systems near the onset of simple (periodic) dynamical instabilities.[2] The present paper represents an improvement of the earlier theory insofar as it includes the presence of nonlinear terms in the equation governing the response to the near-resonant perturbation. We have found that there are two major corrections to the linearized theory. First, the amplitude of the response x is *not* simply proportional to the strength of the input perturbation or signal (see Fig. 5). When operating below the original bifurcation point, the ratio of the output (at the signal frequency) to the input decreases as the input grows larger. This ratio is sometimes called the "gain," and one says here that "the gain saturates" as a function of the input signal strength. When operating above the original bifurcation point, the response can (for small detuning) exhibit a nearly discontinuous change at a critical signal level. This switchlike transition may have *practical applications*; for example, such a system could be used as a sensitive signal detector with an adjustable response threshold, or as an amplifier for digital signals. The second major improvement over the results of the linearized theory is the generation of a symmetrical set of evenly spaced peaks in the power spectrum as the bifurcation point is approached. In contrast, the linearized theory predicts only pairs of lines centered

about $\omega_0/2, 3\omega_0/2, \ldots$.

We would like to close by discussing briefly these two nonlinear effects in the context of a specific application, namely, the superconducting Josephson-junction parametric amplifiers. These devices were proposed originally as good candidates for low-dissipation small-signal amplifiers operating in the frequency range of $\sim 10-100$ GHz. While good signal gain has been achieved,[22-25] the development of parametric amplifiers as practical devices has been thwarted by the appearance of a large amount of broadband noise.[26-31] Moreover, the output noise level G_N increases more rapidly than the signal gain G_S, so that the noise temperature $T = G_N/G_S$ is an *increasing* function of G_S. (Typically, one expects an amplifier to have a noise temperature that is independent of G_S.)

Although a variety of explanations have been forwarded, the origin of this noise rise is still an open issue. (For a nice review, see Ref. 28.) We suggest the following scenario leading to a gain-dependent noise rise in paramps.

First of all, the existence of a large gain factor G_S is due to the presence of a dynamical instability nearby in parameter space:[2,28] the closer the bifurcation, the greater the gain. In the linearized theory developed in Ref. 2, the output at the signal frequency ω_1 is proportional to both the input level ϵ and the reciprocal of the bifurcation parameter μ^{-1}. The analogous theory applied to noisy inputs yields a similar scaling for the output level of the broadband spectrum.[14] Consequently, the broadband noise G_N and the signal gain G_S scale identically, so that the linearized theory predicts a noise temperature T which is independent of G_S. However, the results of this paper suggest two effects that would enhance the broadband output relative to the signal frequency output as the bifurcation point is approached. First, the output at μ_1 grows more slowly than the first power of ϵ—that is, the amplifier can saturate. (The idea that saturation is behind the observed noise rise has been forwarded previously by Feldman within the framework of a different theory of parametric amplifier.[32]) Second, the power contained in the closely spaced lines of the spectrum (see Fig. 12) would presumably get smeared out in the presence of some input noise, and this would lead to the broadband noise level G_N increasing more rapidly than that predicted by the linearized theory (for which the spectrum has only the two central peaks). Together, these two effects imply a noise temperature T that increases as the bifurcation point is approached and hence as G_S increases.

Of course the above scenario gives only a qualitative explanation of the noise rise, and must be developed in much greater detail before we can decide whether it is the correct one. Armed with a true theoretical understanding of the noise rise, we can hope to establish the conditions under which the superconducting parametric amplifiers' performance is optimized.

ACKNOWLEDGMENTS

We gratefully acknowledge the invaluable contribution of Bruce McNamara to the early stages of this work, including his ideas concerning the bifurcation shift and the noise rise in Josephson parametric amplifiers, and the development of the Duffing-equation circuit. We are indebted to J. Clarke and R. F. Miracky for first suggesting the potential relevance of our work to the parametric-amplifier noise-rise problem. We also thank D. Belanger, J. Crutchfield, J. Guckenheimer, C. Jeffries, E. Knobloch, B. Rowe, and P. Scott. This work was supported by a grant from the National Science Foundation (No. PHY-81-15541) and by the Director, Office of Energy Research (Office of Basic Energy Sciences, Materials Sciences Division), U.S. Department of Energy under Contract Number DE-AC03-76SF00098. Work at Brookhaven National Laboratory was supported by Division of Materials Sciences of the U.S. Department of Energy under Contract Number DE-AC02-76CH00016.

APPENDIX: DERIVATION OF THE COMPLETE SPECTRUM FOR THREE SPECIAL CASES

The emergence of higher harmonics in the reduced variable $x(t)$ corresponds to the rise of the spectrum of the dynamical variable $\mathbf{X}(t)$—the closely spaced set of peaks discussed in Sec. III E. Examples of the spectrum corresponding to the cases discussed here are given in Sec. VI.

In the quasistatic limit ($\delta/\epsilon^{2/3}$), there are three special values of μ_1 ($=\mu/\epsilon^{2/3}$) for which all Fourier components of $x(t)$ can be derived. They are (1) the unperturbed bifurcation point, $\mu_1=0$; (2) just before the shifted bifurcation point, $\mu_1=\mu_{1B-}$; and (3) just after the shifted bifurcation point, $\mu_1=\mu_{1B+}$. The results are derived for the rescaled variable $x_1(t_1)$ as determined by Eq. (39). For $x_2(t_2)$ divide the results by $\mu_1^{1/2}$. For $x(t)$ multiply by $\epsilon^{1/3}$.

1. $\mu_1=0$

Here Eq. (39) reduces to

$$x_1(t)=\cos^{1/3}(\delta_1 t_1) \tag{A1}$$

and therefore

$$c_n=\frac{1}{2\pi}\int_0^{2\pi}\cos^{1/3}\phi\cos(n\phi)d\phi\ .$$

This integral can be evaluated (use 3.631-9 from Ref. 19) and one obtains

$$c_n=\begin{cases}\dfrac{2^{-1/3}\Gamma(\frac{4}{3})}{\Gamma(\frac{5}{3}+(n-1)/2)\Gamma(\frac{5}{3}-(n+1)/2)} & n \text{ odd} \quad \text{(A2a)}\\ 0 \quad n \text{ even}\ . & \text{(A2b)}\end{cases}$$

The expression for c_1 can be simplified to

$$c_1=\alpha\frac{1}{8\sqrt{3}\pi}\Gamma^3(\tfrac{1}{3})\approx 0.579\,797\,6$$

$$\approx 0.441\,659\,7\alpha\ , \tag{A3}$$

where $\Gamma(\frac{1}{3})\approx 2.678\,938\,5$ and $\alpha=4^{1/3}27^{1/2}/2\pi \approx 1.312\,769\,2$ and the other cases can be obtained by a re-

cursion relation:

$$c_n = -c_{n-2}\frac{(3n-7)}{(1+3n)} \quad n \text{ odd} . \tag{A4}$$

Thus $c_3 = -\frac{1}{5}c_1$, $c_5 = \frac{1}{10}c_1$, $c_7 = -\frac{7}{110}c_1$, etc.

2. $\mu_1 = \mu_{1B-}$

Since $\mu_{1B} = 3/4^{1/3}$, the equation becomes

$$x_1^3 - (3/4^{1/3})x_1 = \cos(\delta t) . \tag{A5}$$

This cubic is easily solved by standard techniques yielding

$$x_1(t) = \begin{cases} 4^{1/3}\cos(\phi/3) & 0 < \phi < \pi \\ -4^{1/3}\cos(\phi/3 - \pi/3), & \pi < \phi < 2\pi \end{cases} \tag{A6}$$

where $\phi = \delta t \pmod{2\pi}$.

Define P as

$$P = \frac{1}{2\pi}\int_0^{\pi}[4^{1/3}\cos(\phi/3)]e^{-in\phi} . \tag{A7}$$

This is one piece of the integral for c_n, covering the interval from the positive jump in $x(\phi)$ at $\phi = 0$ to the negative one at $\phi = \pi$. P is easily evaluated:

$$P = \begin{cases} \frac{\alpha}{2}\dfrac{1-27^{1/2}ni}{9n^2-1}, & n \text{ odd} \quad \text{(A8a)} \\ \frac{\alpha}{2}\dfrac{-1+3^{1/2}ni}{9n^2-1}, & n \text{ even} . \quad \text{(A8b)} \end{cases}$$

From the symmetry $x_1(t) = -x_1(t - \pi/\delta)$ we obtain c_n:

$$c_n = \begin{cases} 2P = \alpha\dfrac{1-27^{1/2}ni}{9n^2-1}, & n \text{ odd} \quad \text{(A9a)} \\ P - P = 0, & n \text{ even} . \quad \text{(A9b)} \end{cases}$$

$$|c_n| = \alpha\frac{(1+27n^2)^{1/2}}{|9n^2-1|}, \quad n \text{ odd} \tag{A9c}$$

From the expression for $|c_n|$ one can see that asymptotically the amplitudes fall off like $1/n$ as expected for a function with a square-wave character.

3. $\mu_1 = \mu_{1B+}$

Here there are two solutions for $x_1(t)$. The governing equation is the same as the previous case, i.e., Eq. (A5), but now we assume that the transitions do not occur [we can do this because μ_{1B} is the boundary between the square-wave and continuous types of behavior for $x_1(t)$]. There are two stable solutions for $x_1(t)$—x_{1+} and x_{1-}:

$$x_{1+}(t) = \begin{cases} 4^{1/3}\cos(\phi/3), & 0 < \phi < \pi \\ -4^{1/3}\cos(\phi/3 + \pi/3), & \pi < \phi < 2\pi \end{cases} \tag{A10}$$

where $\phi = \delta t \pmod{2\pi}$, and

$$x_{1-}(t) = -x_{1+}(t + \pi/\delta) . \tag{A11}$$

The Fourier coefficients can be expressed in terms of the integral P used in the previous case. We now use the symmetry $x_1(t) = x_1((2\pi/\delta) - t)$ to obtain

$$c_{n+} = P + P^* = -\alpha\frac{(-1)^n}{9n^2-1} , \tag{A12}$$

$$c_{n-} = -(-1)^n c_{n+} = \alpha\frac{1}{9n^2-1} . \tag{A13}$$

---

*Present address.

[1]J. Heldstab, H. Thomas, T. Geisel, and G. Radons, Z. Phys. B **50**, 141 (1983).

[2]K. Wiesenfeld and B. McNamara, Phys. Rev. Lett. **55**, 13 (1985); Phys. Rev. A **33**, 629 (1986).

[3]B. Derighetti, M. Ravani, R. Stoop, P. F. Meier, E. Brun, and R. Badii, Phys. Rev. Lett. **55**, 1746 (1985).

[4]W. Horsthemke and M. Malek-Mansour, Z. Phys. B **24**, 307 (1976); W. Horsthemke and R. Lefever, *Noise-Induced Transitions* (Springer-Verlag, Berlin, 1984).

[5]S. Kabashima, Ann. Israel Phys. Soc. **2**, 710 (1978); S. Kabashima and T. Kawakubo, Phys. Lett. **70A**, 375 (1979); J. Smythe, F. Moss, and P. V. E. McClintock, Phys. Rev. Lett. **51**, 1062 (1983).

[6]K. H. Hoffmann, Z. Phys. B **49**, 245 (1982).

[7]L. Arnold, H. Crauel, and V. Wihstutz, SIAM J. Control Optim. **21**, 451 (1983); L. Arnold, in *Fluctuations and Sensitivity in Nonequilibrium Systems,* edited by W. Horsthemke and D. K. Kondepudi (Springer, Berlin, 1984).

[8]See, e.g., J. Walker, *The Flying Circus of Physics* (Wiley, New York, 1975), p. 39, and references therein.

[9]S. M. Meerkov, in *Fluctuations and Sensitivity in Nonequilibrium Systems,* edited by W. Horsthemke and D. K. Kondepudi (Springer, Berlin, 1984); J. Math. Anal. Appl. **98**, 408 (1984); Diff. Eqs. **9**, 1239 (1973).

[10]S. Rosenblat and G. A. Tanaka, Phys. Fluids **14**, 1319 (1971); G. Venezian, J. Fluid Mech. **35**, 243 (1969).

[11]M. Lücke and F. Schank, Phys. Rev. Lett. **54**, 1465 (1985).

[12]See, e.g., J. P. Crutchfield, J. D. Farmer, and B. A. Huberman, Phys. Rep. **92**, 45 (1982); G. Meyer-Kress and H. Haken, Phys. Lett. **82A**, 151 (1981); J.-P. Eckmann, L. Thomas, and P. Wittwer, J. Phys. A **14**, 3153 (1982).

[13]J. P. Crutchfield and B. A. Huberman, Phys. Lett. **77A**, 407 (1980).

[14]K. Wiesenfeld, J. Stat. Phys. **38**, 1071 (1985); C. D. Jeffries and K. Wiesenfeld, Phys. Rev. A **31**, 1077 (1985).

[15]J. Guckenheimer and P. Holmes, *Nonlinear Oscillations, Dynamical Systems, and Bifurcations of Vector Fields*

(Springer-Verlag, New York, 1983).
[16]P. Bryant and C. Jeffries, Phys. Rev. Lett. **53**, 250 (1984).
[17]D. Jordan and P. Smith, *Nonlinear Ordinary Differential Equations* (Clarendon, Oxford, 1977).
[18]In a supercritical period-doubling bifurcation, a stable period-doubled orbit emerges (continuously) from the periodic orbit as the bifurcation point is crossed. The opposite type, a subcritical bifurcation, involves an unstable period-doubled orbit. This unstable orbit merges with the coexisting stable periodic orbit and an unstable periodic orbit results. Experimentally, one observes a discontinuous (and hysteretic) jump at this point to some coexisting attractor, which could, for example, be a large-amplitude period-doubled orbit. If such discontinuities occur (in the absence of a perturbation), the bifurcation is subcritical and the sign of the cubic term in the normal form [Eq. (2)] must be changed. This will result in a sign change for the bifurcation shift, as well as numerous other effects. Conversely, a continuous bifurcation (without jumps) generally denotes a supercritical bifurcation.
[19]I. S. Gradshteyn and I. M. Ryzhik, *Table of Integrals, Series and Products* (Academic, New York, 1980).
[20]J. E. Marsden and M. McCracken, *The Hopf Bifurcation and Its Applications* (Springer-Verlag, New York, 1976).
[21]This assumes a nondegenerate bifurcation of the supercritical type, see Ref. 18.
[22]M. J. Feldman, P. T. Parrish, and R. Y. Chiao, J. Appl. Phys. **46**, 4031 (1975).
[23]Y. Taur and P. L. Richards, J. Appl. Phys. **48**, 1321 (1977).
[24]J. Mygind, N. F. Pedersen, O. H. Soerensen, B. Dueholm, and M. T. Levinsen, Appl. Phys. Lett. **35**, 91 (1979).
[25]M. T. Levinsen, N. F. Pedersen, O. H. Soerensen, B. Dueholm, and J. Mygind, IEEE Trans. Electron. Devices **ED-27**, 1928 (1980).
[26]R. Y. Chiao, M. J. Feldman, D. W. Petersen, B. A. Tucker, and M. T. Levinsen, in *Future Trends in Superconductive Electronics (Charlottesville, 1978)*, edited by B. S. Deaver, Jr., C. M. Falco, J. H. Harris, and S. A. Wolf (AIP, New York, 1978), p. 259.
[27]B. A. Huberman, J. P. Crutchfield, and N. H. Packard, Appl. Phys. Lett. **37**, 750 (1980).
[28]M. J. Feldman and M. T. Levinsen, IEEE Trans. Magn. **MAG-17**, 834 (1981).
[29]N. F. Pedersen and A. Davidson, Appl. Phys. Lett. **39**, 830 (1981).
[30]M. T. Levinsen, J. Appl. Phys. **53**, 4294 (1982).
[31]R. F. Miracky and J. Clarke, Appl. Phys. Lett. **43**, 508 (1983).
[32]M. J. Feldman, J. Appl. Phys. **48**, 1301 (1977).